# Oxide-based RRAM materials for neuromorphic computing

**XiaoLiang Hong, Desmond JiaJun Loy, Putu Andhita Dananjaya, Funan Tan, CheeMang Ng & WenSiang Lew**

**Journal of Materials Science**
Full Set - Includes `Journal of Materials Science Letters'

ISSN 0022-2461
Volume 53
Number 12

J Mater Sci (2018) 53:8720-8746
DOI 10.1007/s10853-018-2134-6

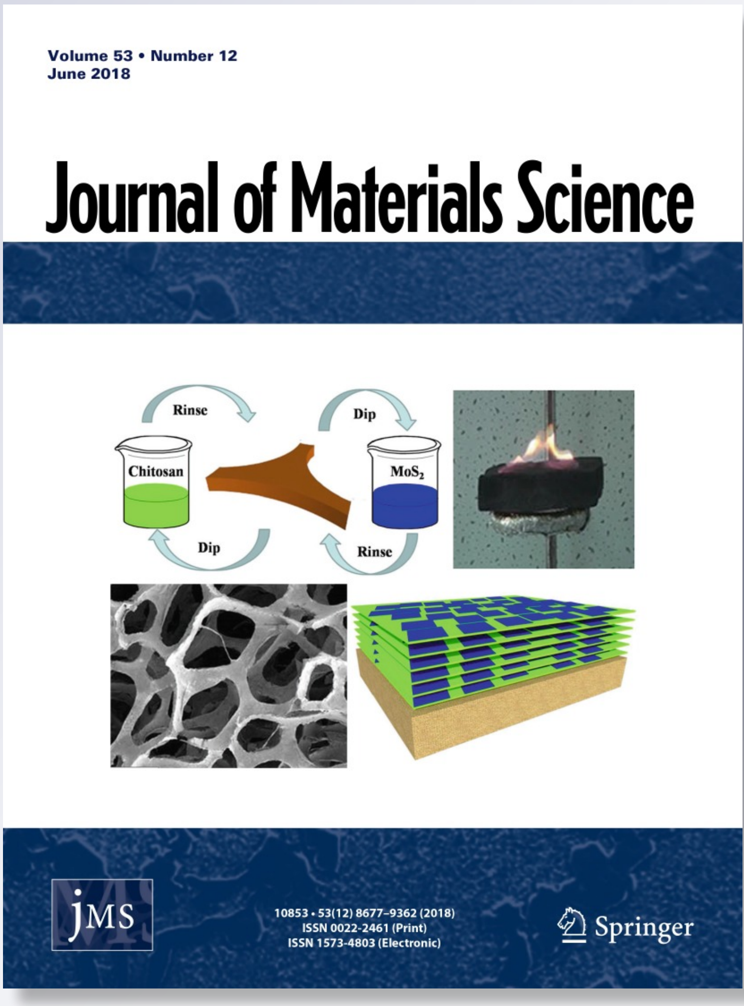


Springer

*J Mater Sci* (2018) 53:8720–8746

**Review**

# Oxide-based RRAM materials for neuromorphic computing

XiaoLiang Hong[1], Desmond JiaJun Loy[1], Putu Andhita Dananjaya[1], Funan Tan[1], CheeMang Ng[2], and WenSiang Lew[1,*]

[1] *Division of Physics and Applied Physics, School of Physical and Mathematical Sciences, Nanyang Technological University, 21 Nanyang Link, Singapore 637371, Singapore*

[2] *School of Electrical and Electronic Engineering, Nanyang Technological University, 21 Nanyang Link, Singapore 637371, Singapore*

**Received:** 27 October 2017

**Accepted:** 10 February 2018

**Published online:** 20 February 2018



## ABSTRACT

In this review, a comprehensive survey of different oxide-based resistive random-access memories (RRAMs) for neuromorphic computing is provided. We begin with the history of RRAM development, physical mechanism of conduction, fundamental of neuromorphic computing, followed by a review of a variety of RRAM oxide materials (PCMO, $HfO_x$, $TaO_x$, $TiO_x$, $NiO_x$, etc.) with a focus on their application for neuromorphic computing. Our goal is to give a broad review of oxide-based RRAM materials that can be adapted to neuromorphic computing and to help further ongoing research in the field.

## Introduction

Resistive random-access memory (RRAM) utilizes the resistive switching (RS) phenomena to store information, which offers new types of devices that can outstrip the performance of traditional semiconductor electronics devices. Compared to charge-based memory devices, RRAM stands out due to its smaller cell size $4F^2$, multi-bit capability as well as energy per bit ($\sim$ fJ/bit). The first report of resistive switching phenomena is by Hickmott [1], where resistive switching is found on $SiO_x$, $Al_2O_3$, $Ta_2O_5$, $ZrO_2$ and $TiO_2$. However, it was only after 38 years that the heat of RRAM research was reawakened with the observation of resistive switching behavior in magnetoresistive films from University of Houston [2]. Two years later, 64-bit RRAM array using $Pr_{0.7}Ca_{0.3}MnO_3$ via a 500-nm complementary metal oxide semiconductor (CMOS) process was reported by Zhuang [3]. Between 2004 and 2007, Samsung and Infineon [4] made a significant progress on RRAM development with the first 3D RRAM array demonstrated in 2007. The concept of RRAM used for neural network and logic circuit was first published in *Nature* by HP in 2008. The paper titled "The Missing Memristor Found" [5] triggered another heat of RRAM development. In the next 9 years, great achievement had been witnessed from industries and academies. The successful fabrication of 64-MB RRAM test chip, 32-Gbit bilayer cross-point RRAM, 27-nm 16-Gbit Cu-based CBRRAM test chip and 4-layer 3D vertical self-selective RRAM array was

Address correspondence to E-mail: wensiang@ntu.edu.sg



https://doi.org/10.1007/s10853-018-2134-6

announced by Unity [6], SanDisk/Toshiba [7], Micron/Sony [8] and IMECAS [9], respectively. In 2017, TSMC [10] announced its new plan to start producing embedded RRAM chips in 2019 using a 22-nm process. Figure 1 shows the historical timeline of important events on RRAM development in the last half-century.

RRAM technology is compatible to the conventional CMOS in a simple way [11], and the RRAM embedded system could be integrated into IoTs, automobile and infotainment platforms [12, 13]. In addition to the memory hierarchy, RRAM has demonstrated its application in the low-power computing as non-volatile logic circuits and neuromorphic computing as a synaptic device. Recent reviews by H.S.P. Wong, Yu, S. M. and Akinaga, H [14–16] gave excellent and comprehensive overviews of RRAM physical mechanism, materials, performance and applications. Here, we limit this review to the oxide-based RRAM materials where neuromorphic computing applications have been demonstrated. At first, fundamentals of RRAM and neuromorphic computing will be discussed. Thereafter, we will elaborate more on these oxide-based RRAM devices (PCMO, $HfO_x$, $TaO_x$, $TiO_x$, etc.) used for neuromorphic computing application. This review will end with a conclusion and outlook.

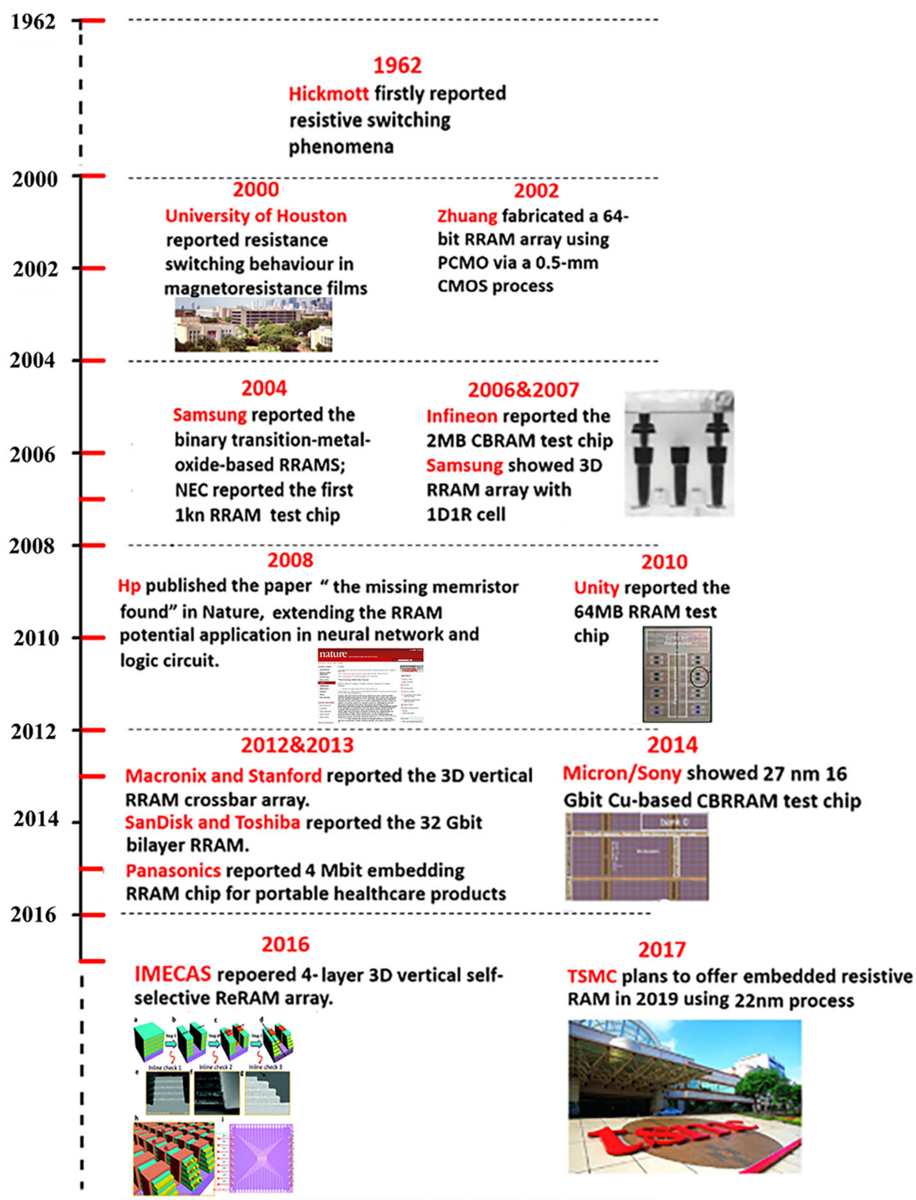


**Figure 1** Historical timeline of RRAM development from 1962 to 2017 [1–10].

## RRAM design and physical mechanism

A typical RRAM structure consists of three layers of materials, namely (metal–insulator–metal) MIM structure [17], which is a resistive oxide layer sandwiched between two electrodes. The resistance of the device can be modulated by applying an external electric field across the electrodes. RRAM devices work based on chemical redox reactions, i.e., oxidation and reduction reactions. In memory storage, there are binary states, "0" and "1". "0" represents data that is not stored, while "1" represents data that is stored. In RRAMs, redox reactions form a filament or bridge across the two metal layers, within the insulator. When a filament is created, an electrically conductive is formed between the two metal layers. Hence, a low-resistance state (LRS) occurs when a filament is formed, while a high-resistance state (HRS) occurs when a filament is not formed or ruptured. When a filament is formed, it would be a "1" state where one bit of information is stored and when a filament is ruptured, it would be a "0" state [18] (Fig. 2). A typical hysteretic current–voltage (*I*–*V*) characteristics in a metal–insulator–metal (MIM) structure are shown in Fig. 3. The switching from HRS to LRS is called the SET process, while the switching from LRS to HRS is called RESET process. In most situations, a forming voltage larger than the SET voltage is needed for the pristine device to trigger the resistive switching behaviors for the subsequent cycles. The SET and RESET processes can occur at the same polarity of the applied voltage as shown in Fig. 3a which is known as unipolar switching. Similarly, bipolar switching refers to the switching behaviors occurring at different polarities of voltage (Fig. 3b).

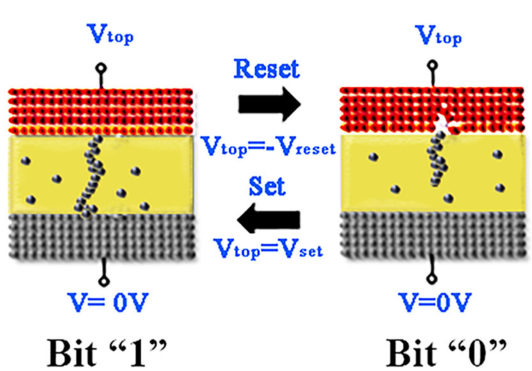


**Figure 2** A schematic diagram of the mechanism of resistive switching effect in RRAM cell, "1" state when a filament is formed and "0" state when a filament is ruptured.

The MIM stack of RRAM can be broadly classified as symmetric and asymmetric structures. A symmetric MIM structure mainly exhibits unipolar switching behavior, while a asymmetric structure mainly exhibits bipolar switching behavior. The mechanism of resistive switching behavior can mainly be classified into the electrochemical metallization effect (ECM) and the valence change memory effect (VCM) [19]. ECM and VCM are typically observed in RRAMs with one active metal electrode (Cu, Ag, Ni) and one inert metal electrode (Pt, Ru, Au or Ir). In ECM, the conductive path of the switching layer is formed via metal cations of the electrochemically active metal electrode under an external electric field. On the other hand, VCM works based on the migration of anions where oxygen vacancies contribute to the conductive path within the oxide layer. In VCM, it typically requires an oxygen scavenging electrode to facilitate anionic movement between the active and inert electrodes. ECM and VCM are based on redox reactions of oxidation and reduction. RRAM devices with switching layer doped with Ti [20] or Ge [21] had been reported to have a forming-free property where their initial resistance state (IRS) is similar to the high-resistance state (HRS). In addition, several other advantages of doping in the RRAM fabrication process to improve uniformity and frustration had been reported [22]. Besides the single switching layer, numerous investigations had been conducted on double and multiple switching layers. It has been reported that a switching layer consisting of low-resistance and high-resistance layers can reduce the randomness of resistive switching. Additionally, multi-layer structures have been promising for the multi-level storage function [23, 24]. Table 1 summarizes the details of the RRAM stack, electrodes and switching layers.

The conduction mechanism in oxide RRAM can be analyzed by fitting the *I*–*V* characteristic of current conduction in the HRS and the LRS. Various resistive switching mechanisms have been proposed to explain and model RRAM conduction behavior. They include the Pool–Frenkel emission (P–F emission), SCLC (spaced charge limited current), formation and rupture of conductive filaments (CFs), electrode-limited conduction (Table 2) [42]. Although the underlying physical mechanisms are material/electrode specific and not well understood, the

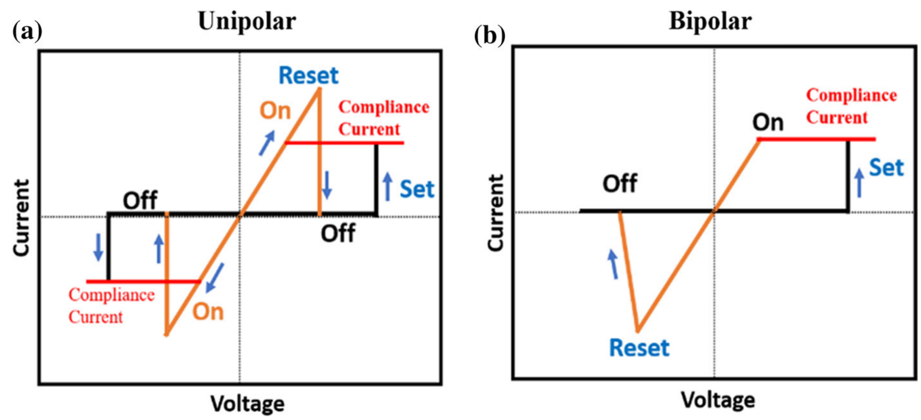


**Figure 3** Typical hysteretic current–voltage (*I*–*V*) characteristics in metal–insulator–metal (MIM) structures **a** unipolar switching and **b** bipolar switching.

conductive filament mechanism applies to a large majority of binary oxide unipolar or bipolar RRAMs.

## Neuromorphic computing

Comparing with traditional computational architecture, the human brain working system has major advantages in the following aspects. The energy efficiency of the human brain (10 watts) [15] is remarkably superior, reaching 5 orders of magnitude lower than supercomputers. The human brain can also adapt to different environments and is able to perform complex processing. The advancement of studies on the human brain system has led to a new disruptive technology neuromorphic computing. This technology imitates how the brain is working in the design and implementation of the computational system.

The ultrahigh energy efficiency of the human brain is derived from its low-power neurons and spike-based computation, which is mainly realized by four components (Fig. 4). Neuron bodies function as an integrator and a device for threshold spiking. In order to implement a neuromorphic system, a capacitor is used to mimic neuron bodies in neuromorphic architecture. Axons work as information transmission connection which could be mimicked a long wire. The signal input from multiple neurons to a single neuron is provided by dendrite, a short wire which plays the role of dendrite in the neuromorphic system. The synapse is the most investigated component that has been constructed so far, and it provides dynamical interconnections between neurons by switching and plasticity. Memristor is the device component that works as a substitution to a synapse. In the neuroscience, synaptic weight of synapse refers to the strength or amplitude of a connection between two neurons which is mainly determined by the amount of neurotransmitter released and absorbed. The synaptic plasticity is the increase or decrease of synaptic weight over the time. Short-term synaptic plasticity acts on a timescale of tens of milliseconds to a few minutes, while long-term plasticity lasts from minutes to hours. Memristors are electrical devices which can mimic the synapse. The resistance of memristors, which functions as the synaptic weight in the neuroscience, can be tuned as response to a periodic voltage (or current) input, and the resistance state can be retained when the power is turned off. RRAM is one form of memristor, and its resistance (synaptic weight) can be manipulated between high and low resistive states by deliberately applied voltage, which causes the medium to acquire microscopic conductive paths called filament. In addition, it is possible to reproduce synaptic plasticity with RRAM memory run by specific coding schemes. In the human brain, 100 billion neurons are connected to one another by 100 trillion synapses [43]. The neuromorphic computing processor consists of a vast array of electronic spiking neurons and multi-bit synapses realized using fully interconnected crossbar memories.

There is a very large amount of fascinating work performed to develop memristors for neuromorphic systems. So far, several types of memristors have been investigated including but not limited to RRAM [44–49], phase change memory [50–61], spin device [62–68], floating gate transistors [69–76] and an optical device [77–81]. Among them, RRAM is an excellent memristor for non-volatile synapse application as it enables higher density, scalability and efficient

**Table 1** Summary of RRAM stack, electrodes and switching layer

| | Structures | Switching behavior | Model |
|---|---|---|---|
| *RRAM stack* | | | |
| Symmetric and asymmetric | Symmetric structure: (e.g., Pt/NiO/Pt [25], Pt/$TiO_2$/Pt [26], Pt/ZrO2/Pt [27], Pt/$HfO_2$/Pt [28]) | Mainly unipolar switching | Thermal dissolution model: Oxygen ions accumulated near the anode during the SET. The Joule heating activates $O^{2-}$ to combine with oxygen vacancies during the RESET and rupture of conductive filaments (CFs) |
| | Asymmetric structure: (e.g., Pt/$TiO_2$/TiN [29], TiN/ZnO/Pt [30], TiN/$HfO_2$/Pt [31], Pt/NiO/Cu [32], Cu/$La_2O_3$/Pt [33]) | Mainly bipolar switching | Ionic migration model: Oxide interfacial layer formation between electrode and oxide acts as oxygen diffusion barrier. |

| | Structures | Mechanism | Advantages |
|---|---|---|---|
| *RRAM electrodes* | | | |
| Active and inert metal electrode | Active metal electrode: Ti, Al, Ag, Cu, Ni, TiN, TaN, ZrNx, ITO | ECM VCM Mainly bipolar switching | Active + inert electrodes in RRAM exhibit better endurance and longer retention time |
| | Inert metal electrode: Pt, Au, Ru, Pd | VCM Mainly unipolar switching | |
| | Novel electrodes: CNT [34, 35] n + Si [36] graphene [37] | | n + -Si: self-rectifying property which is capable of alleviating cross talk issues<br>Graphene and carbon nanotube electrodes: ultradense memories. |

| | Structures | Mechanism | Advantages |
|---|---|---|---|
| *RRAM switching layer* | | | |
| Doping | Dopants: Ti [20], Ge [21] | Forming-free: Dopants diffuse into oxide layer and oxygen vacancies are increased | Good data retention, potential multi-bit operation, highly scalable property and fast switching speed<br>Better uniformity (temporal fluctuations) (cycle to cycle) and spatial fluctuations (device to device) |
| Bilayer | One layer with lower resistivity and one with higher resistivity E.g., $TMO_1/TMO_2$ [24], Ni/$GeO_x$/HfOx/TaN [38], MoOx/GdOx [39] | Resistive switching occurs at higher resistivity layer, and the lower resistivity layer can improve the resistance of the ON state | Low power consumption<br>Lower RESET current<br>Better uniformity (diffusion of metal ions from the lower resistivity to the higher resistivity layer. This stabilizes the CFs to reduce the randomness of resistive switching (RS) |
| Multi-layer | E.g., Pt/$HfO_x$/$TiO_x$/$HfO_x$/$TiO_x$/TiN [40]., Pt/$Ta_2O_5$/$TiO_xN_y$/TiN/$Ta_5$/Pt [41] | | Multi-level storage function |

chip design. When compared with other types of synaptic device, RRAM possesses the advantages of high endurance that FLASH memories do not offer, lower programming energy and smaller cell size than MRAM. In addition, the non-volatile property of RRAM outweighs the traditional DRAM which requires constant recharging [82–87]. Table 3 lists out some of the leading institutions and industries using

**Table 2** Conduction mechanism analysis

| Mechanism | Remarks |
|---|---|
| P-F emission (field-assisted thermal ionization) | Thermal excitation of electrons emits from traps into the conduction band of the dielectric. $\ln(1/V) - V^{1/2}$ |
| SCLC (space charge limited current) | When electric field is high, the current is dominated by the charge carrier injected from the electrode. The current is only dependent on the mobility rather than the charge-carrier density. $I$–$V^2$ |
| Conductive filament | Formation and rupture of conductive filaments $I$–$V$ Not proportional to electrode area |
| Electrode limited | Relevant to electrode (materials, area) |
| Schottky emission | Thermal excitation of electrons emits over the barrier into the conduction band of the dielectric. |
| Direct tunneling | Electron tunnels from cathode to anode directly Thin film thickness less than 3 nm |
| Fowler–Nordheim (F-N) tunneling | Electron tunnel from cathode to conduction band directly High voltage |

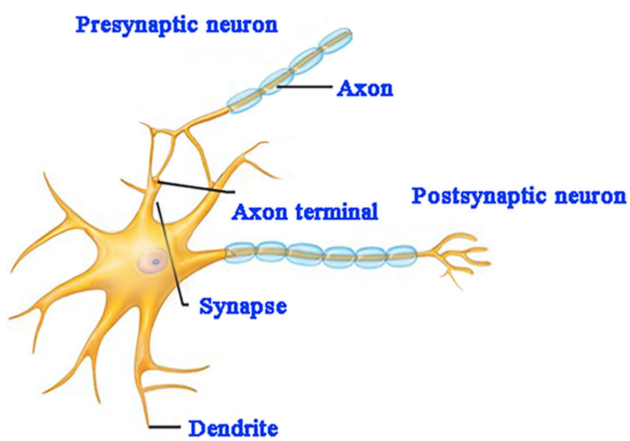


**Figure 4** Interconnectivity in neuronal circuit.

resistive memories as synaptic devices. Phase change memory (PCM) has shown great potential for neuromorphic computing in the Synapse project performed by leading researchers from IBM (TrueNorth) [88]. However, the greatest drawback is its high power consumption. RRAM is touted as a possible solution and has been studied by Nanoelectronics and Nanotechnology Research Group from Stanford University and NanoST laboratory from National Chiao Tung University [89–92]. The results showed that RRAM possesses similar performance as that of PCRAM and consumes less power to operate artificial synapse [93–95]. Since then, RRAM has attracted massive attention from numerous academic institutions. From Fig. 5, the number of publications on RRAM has increased by 14 times in the last decade. Among these publications, the proportion of papers demonstrating neuromorphic computing applications has increased every year since 2010. In 2016, nearly 11% of papers presented RRAM's applications in the neuromorphic system. In general, most of studies on RRAM involve oxide materials. Oxide-based RRAM is attractive as the underlying metal insulator–metal structure is simple, compact and CMOS-compatible. Most importantly, the multi-level behavior needed to imitate adaptive synaptic changes

**Table 3** Active players in the resistive memory of the synaptic devices (with to Ref. [97])

| Project performer | Synaptic device | Device structure | Scale | Synaptic characteristics | Application |
|---|---|---|---|---|---|
| GIST | RRAM | $TiO_x/HfO_x$ | Unit cell | Multi-level cell | Visual cortex |
| LETI | CBRAM | $Ag/GeS_2$ | 8 × 8 1T1R | N/A | Human Cochlea and Retina |
| Stanford | PCM | GST | 10 × 10 1T1R | Yes | Pattern recognition |
| POSTCH | RRAM | $Pr_{1-x}Ca_xMnO_3$ | 11 k Array | Yes | Signal recognition |
| IBM | PCM | $Ge_2Sb_2Te_5$ | 165 K Array | N/A | Pattern recognition |

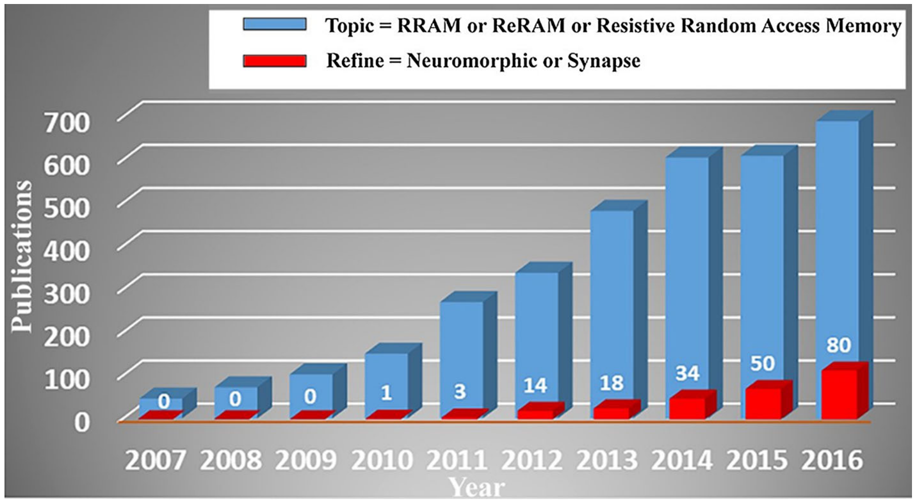


**Figure 5** Publications per year from 2007 to 2016. The data is from the web of science site (www.webofknowledge.com). The search expression for blue bars is Topic = "R-RAM" or "RRAM" or "Resistive random-access memory". The data for red bars are from subsequent refined with expressions Refine = "neuromorphic" or "synapse".

has been found in many oxide-based RRAM devices. In addition, the energy per synaptic operation can be made as low as sub-pJ and the programming current can reach below 1 μA [96]. In this review, we will focus on oxide-based RRAM memristor device as a synapse in the neuromorphic system.

The basis of learning and formation of memory are the modification of synapse connections as a result of accumulated experience, the feature known as synaptic plasticity. So far, synaptic plasticity had been widely studied their correlation in learning and memory [98–100]. Hebbin's rule postulates that changes at synapses within the brain underlie learning and memory, which was proposed by Donald Hebb in 1949 [101]. It provides an algorithm to update weight of neuronal connection within neural network and a physiology-based model to reproduce the activity-dependent features of synaptic plasticity. In biology, excitatory and inhibitory postsynaptic potentials are transmitted between neurons through chemical and electrical messaging at synapses, driving the generation of the new action potentials (spikes). In RRAM-based neuromorphic approaches, the tunable resistive state of RRAM functions as synaptic weight in the neuromorphic system. The weight of synapse could be manipulated by changing the resistance states in RRAM devices, which follows the rule of spike-timing-dependent plasticity (STDP) [102–104]. STDP is a form of synaptic plasticity that adjusts the strength of the connection between the presynaptic neuron and postsynaptic neuron based on the relative timing of its output and input action potentials (electric pulses). In the implementation of STDP learning rule, it requires the adjustment of the connection strength between pre- and postsynaptic neurons. The process of adjusting the strength of these interneural connections is known as synaptic operation. The number of synaptic operations of a neuromorphic chip is strongly dependent on the intrinsic properties of the materials used as the synapse. This will further determine the lifetime of the chip or its availability for learning process. The required cyclability (number of synaptic operations) of the chip will depend on the expected lifetime and operation frequency of the chip. If the chip is expected to be available for learning for about 10 years under 100 Hz of operation frequency, the chip must be able to execute at least $10^{10}$ synaptic operations. RRAM device has been reported to achieve endurance of as high as $10^{12}$; thus, it emerges as one of the strongest candidates for the development of highly reliable neuromorphic chip. The feasibility of RRAM device for synapse applications was first demonstrated in 2010 by Jo et al. [53]. According to the experimental RRAM STDP curve as shown in Fig. 6, conductance increases with the time delay when the presynaptic spikes precede the postsynaptic spikes ($t < 0$). Conversely, the decrease of conductance occurs when the postsynaptic spikes precede the presynaptic spikes ($t > 0$). In addition to the rise/fall of synaptic weight, the change of synaptic weight could also be either long term or short term. Upon changing the spike rate, Ohno [105] demonstrated both the long-term potentiation and short-term potentiation in $Ag_2S$-based RRAM device. Long-term potentiation refers to the persistent increase in synaptic strength which lasts minutes or more, while short-term potentiation refers to the transiently

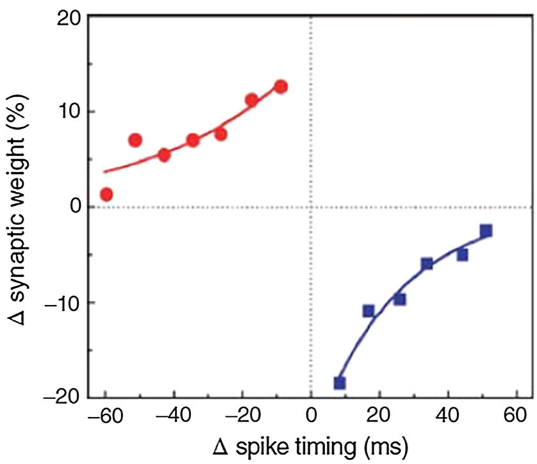


**Figure 6** Experimental RRAM STDP curve. (Reprinted with permission from Ref. [53].).

enhancement of synaptic strength which acts on a timescale of tens of milliseconds to a few minutes. The results showed that the RRAM device exhibits short-term potentiation behavior with the applied pulse width at 0.5 s and interpulse delay at 20 s. As shown in Fig. 7, the potentiation of synaptic weights is volatile and no permanent change was observed after nine pulses. However, when the interpulse delay was reduced by 10 times, 6 pulses are sufficient to induce the stable potentiation and permanent high conduction state remains thereafter. In general, short-term and long-term plasticity could be mimicked in the single synapse by tuning the non-overlapping spike rate. This synaptic plasticity plays a crucial role in the way the brain implements learning and memory. Therefore, the rule of STDP (Fig. 7) is considered as one implementation of Hebbian learning.

## Oxide-based RRAM for neuromorphic computing application

Resistive switching behavior had been observed in many oxides, while most of them are transition metals. Some of them had been explored for neuromorphic application and summarized in the periodic table (Fig. 8). We selected PMCO, $HfO_x$, $TaO_x$, $TiO_x$, $NiO_x$, $AlO_x$, $WO_x$ and other oxides for discussion in this article as their property and application for neuromorphic computing were well investigated. The growth techniques of RRAM oxide materials include traditional deposition methods, i.e., sputtering, atomic layer deposition (ALD) and pulsed laser deposition (PLD). In addition, novel methods for RRAM fabrication have also been reported. The traditional and novel methods for RRAM are listed in Table 4.

### $Pr_{1-x}Ca_xMnO_3$ (PCMO)-based synaptic devices

$Pr_{1-x}Ca_xMnO_3$ (PCMO), as representative materials in perovskite transition metal oxide, has been widely employed as synaptic devices. Its resistive switching property was first discovered by Asamitsu et al. in late 1990 [135], which draws the attention from academies on complex transition metal oxide for RRAM device [136, 137]. The resistive switching of PCMO is based on metal–insulator (MIT) mechanism. MIT is a kind of valence change system, in which the electrons are injected into the insulator layer to conduct the current with an external applied field. In PCMO, the injected electronic charge distorts the superlattice structure and the mixed valence band behavior, a

**Figure 7** **a** Short-term potentiation and **b** long-term potentiation of $Ag_2S$-based devices are induced for different spike rates. (Reprinted with permission from Ref [105].).

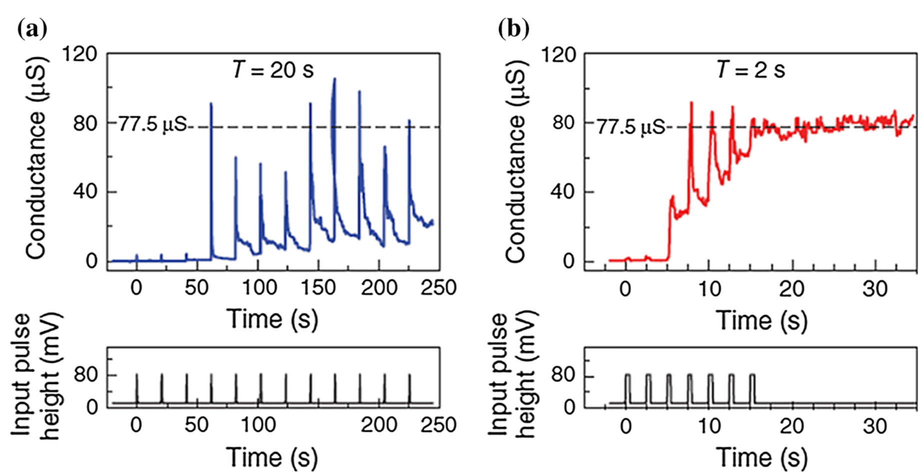

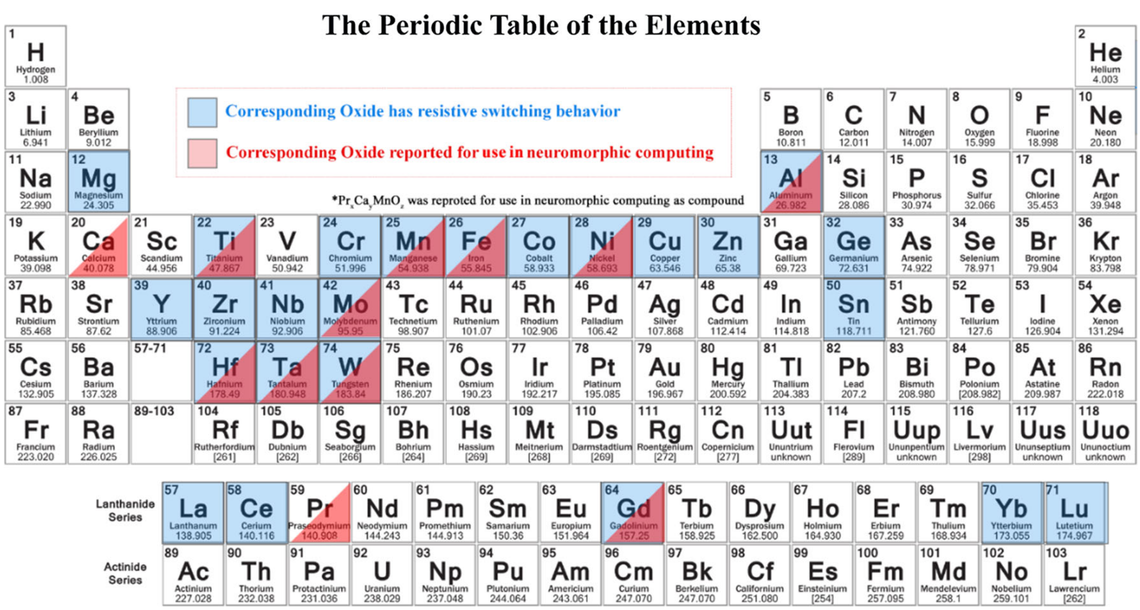


**Figure 8** The periodic table of the elements highlighted with the host metal of RRAM materials and those had demonstrated for neuromorphic computing.

**Table 4** Summary of RRAM device fabrication methods

| *RRAM device deposition methods* | |
|---|---|
| Traditional methods | Sputtering [106–113] |
| | Atomic layer deposition [23, 114–117] |
| | Pulsed laser deposition [118–122] |
| | Plasma enhanced chemical vapor deposition [123–125] |
| | Chemical synthesis particle + spin-coating [126–128] |
| | Sol–gel [129–132] |
| Novel methods | Shattering process using an atomic force microscopy (AFM) tip [133] |
| | Semi-auto screen printer [134] |

process similar to ion doping processes. In addition, PCMO is LRS active materials in which the SET operation is associated with reverse biasing, while RESET operation occurs at forward biasing.

In 2012 and 2013, Park [138, 139] demonstrated 1-kbit cross-point array neuromorphic system based on PCMO synaptic devices. The HRS is achieved with the applied positive bias when the oxygen ions are attracted from the PCMO layer, thus forming a thicker oxide layer with Al electrode. The continuously increasing potentiation and depression behaviors were found when the identical spikes (pulses with same amplitude and width) were applied. In order to overcome the difficulty in achieving gradual long-term depression (LTD) caused by asymmetry potentiation/depression, a new programming scheme was developed [140]. The growth process control of PCMO device with TiN electrode was studied to optimize the device electric performance [141]. Similarly, to avoid an abrupt LTD, a two-PCMO-memristor device model was proposed by Moon et al. [142]. In 2015, a circuit capable of realizing the learning process was designed and published [143]. In the same year, a high-density PCMO cross-point synapse array on the 8-inch wafer was fabricated. The proposed system had been demonstrated to recognize human thought patterns for three vowels [97]. In addition, vivo experiment had also been performed by the group. In the paper, the PCMO-based nanoscale analogy synapse device was successfully applied for neural fear-conditioning signal recognition on a live rat. In 2016, Moon, K from Hwang, H group reported PCMO-based interface switching device with 5-b MLC (32 levels) and improved data retention by using Mo electrodes for the neuromorphic system [144]. The Mo/PCMO synapse array has experimentally confirmed with the realization of pattern recognition with high accuracy when working with $NbO_2$ oscillator neuron [145]. In 2017, a comprehensive study of PCMO-based synaptic devices had been reported in the book "Neuro-inspired Computing Using Resistive Synaptic Devices" [146]. The PCMO synapse performance is evaluated in 1-kb and 8-kb crossbar arrays. The interfacial-type PCMO RRAM was demonstrated with wide on/off ratio ($10^4$), extremely stable analogy resistance changes and low LRS current (1 μA) when device scales down to 150 nm. The influence of active electrode, nitrogen treatment and extra insulating layer ($AlO_x$) has also been investigated. The synaptic performance of PCMO is evaluated as shown in Fig. 9, where the potentiation and depression with identical and non-identical spikes are displayed. It is observed that the gradual switching of depression is only triggered by non-identical spikes, which is accounted for the high asymmetry ratio of potentiation/depression conduction.

So far, PCMO is one of the most matured RRAM materials for neuromorphic computing. It possesses various advantages: nanoscale device dimension (150 nm), multi-level states (5-b MLC), retention, uniformity (STD($\sigma$)/$I_{ave}$ < 0.5), on/off ratio ($10^4$) and high-density crossbar array structure (8 kb) [146]. However, further improvement of symmetric weight update is still required.

## $HfO_x$-based synaptic devices

$HfO_x$ materials have been widely used in RRAM materials because of its excellent CMOS compatibility. In industries, $HfO_x$ has been employed as a high-k dielectric for the gate insulator of CMOS MOSFETs. In $HfO_x$-based RRAM device, TiN is usually applied as an electrode. TiN functions as an oxygen scavenger that depletes the O atom from $HfO_x$ thin film and functions as an oxygen reservoir. It has been reported that $HfO_x$ RRAM has a large on/off ratio (> $10^2$), high endurance (> $10^6$), retention, multi-bit storage and high-speed operation (< 10 ns) [142–146].

In 2011, a novel electronic synapse of $HfO_x$/$AlO_x$-based memory was presented by Yu et al. The structure showed attractive features such as reduced randomness of resistive switching, multi-level switching and the capability to modulate resistances based on the input pulse amplitudes, suggesting great potential to use in emerging neuromorphic computation system [147]. In 2012, the same group reported $HfO_x$-based RRAM device application in the neuromorphic visual system. At the system level, a neuromorphic visual system consisting of 1024 CMOS neuron circuits and 16,348 RRAM synaptic devices was fabricated. The system exhibited great performance in image orientation selectivity and high tolerance on temporal and spatial variability. After one year, Gao, B [148] and his coworkers developed a method to achieve gradual switching on the setting process in TiN/HfOx/Pt devices. To avoid the generation of random and avalanching oxygen vacancies

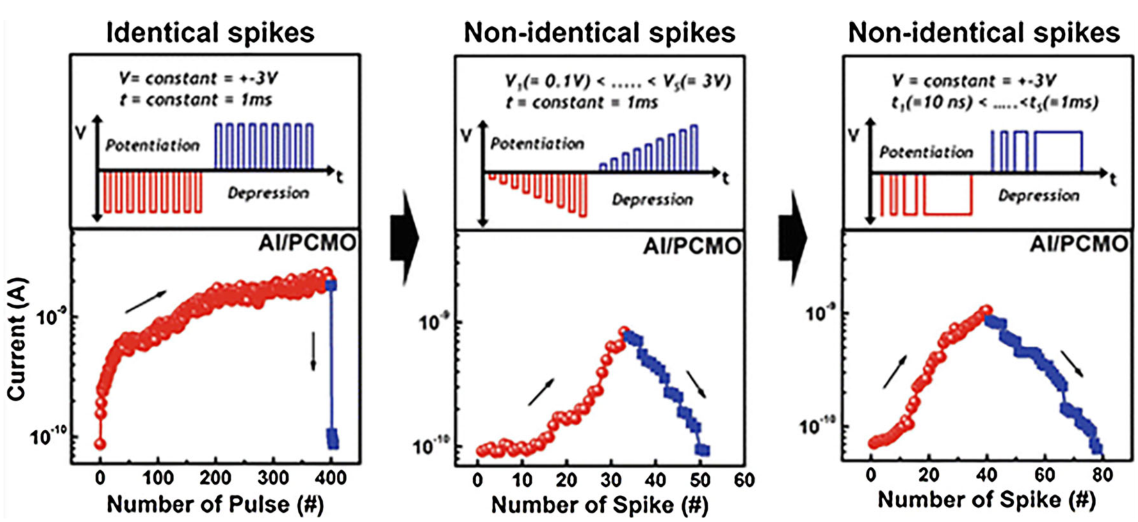


**Figure 9** Potentiation and depression with various programming spikes: identical and non-identical spikes, reprinted with permission from Ref. [146].

($V_O$) clusters, the team developed a methodology by doping trivalent elements into $HfO_x$ layer. The local formation energy of $V_O$ near the dopants was reduced, and $V_O$ will distribute more uniformly in the conductive filament region. The fabricated TiN/Gd:$HfO_x$/Pt devices have also shown controllable multilevel resistive switching behavior. Garbin [149] applied pulse-train schemes to a 3 bit per cell $HfO_2$ RRAM in 2014, causing the relative standard deviations of resistance levels to improve up to 80% compared to the single-pulse scheme. In the same year, Benoist, A integrated TiN/$HfO_2$/Ti/TiN RRAM with an advanced 28-nm CMOS process [150]. A global overview of $HfO_2$ material performances was assessed on a statistical basis, and projection for larger array integration was discussed. The influence of Cu dopant was investigated by Tingting, G., and it was found that Cu-doped $HfO_2$-based RRAM has improved resistive switching with multilevel storage [151]. The application of Mn-doped $HfO_2$-based RRAM has demonstrated speech recognition by Mandal [3]. A comparison between a 20-nm times 20-nm sized synaptic memory device with that of a state-of-the-art VLSI SRAM synapse has exhibited $10^3$ reduction in area and $10^6$ times reduction in the power consumption per learning cycle. The colormap for speech recognition of words "Hello" and "Apple" is shown in Fig. 10.

In 2015, Wang presented a new artificial synapse scheme, consisting of a $HfO_x$ RRAM memristive switches connected to 2 transistors responsible for gating communication and learning operations. STDP was achieved through appropriate shaping of the presynaptic and the postsynaptic spikes [152]. Covi, E demonstrated the Al:$HfO_2$ memristor device use for artificial synapse, emulating the potentiation and depression processes using an easily implementable algorithm based on a train of identical pulses [153]. The impact of $HfO_x$-based synapses cycle to cycle (temporal) and device to device (spatial) variability on the convolutional neural network was investigated by Garbin, D [154]. The results showed that the convolutional neural network (CNN) architecture has a high tolerance to the variability. Lee et al. [155] proposed a silicon-based charge trap memory with Al/$HfO_2$/$Al_2O_3$/$Si_3N_4$/Si structure. The device implemented both short-term plasticity and long-term potentiation in the synapse. The use of $HfO_2$-based oxide-based resistive memory (OxRAM) devices operated in a binary mode to implement synapses in a CNN was also studied by Garbin, D in 2015 [149]. The proposed $HfO_2$-based OxRAM technology offers good electrical properties including high endurance ($> 10^8$ cycles), fast speed ($< 10$ ns) and low energy ($< 10$ pJ). High accuracy (recognition rate $> 98\%$) was demonstrated for a complex visual pattern recognition application. Covi, E proposed TiN/$HfO_2$/Ti/TiN memristor as artificial synapse for neuromorphic architectures. The collected STDP data were used to simulate a simple fully connected spiking neural network (SNN) for pattern recognition [156]. An innovative approach for real-time decoding of brain signals based on SNN was presented by Werner [157]. $HfO_X$-based RRAM devices were used to implement synapse and SNN, enabling the network for autonomous online spike sorting of measured biological signals. The system allows real-time learning and completely unsupervised operation. The real-time functionality, low power consumption (10 nW) and high recognition rate 90% of the system make it a great candidate for future healthcare applications. $HfO_x$-based synapses were used in SNN

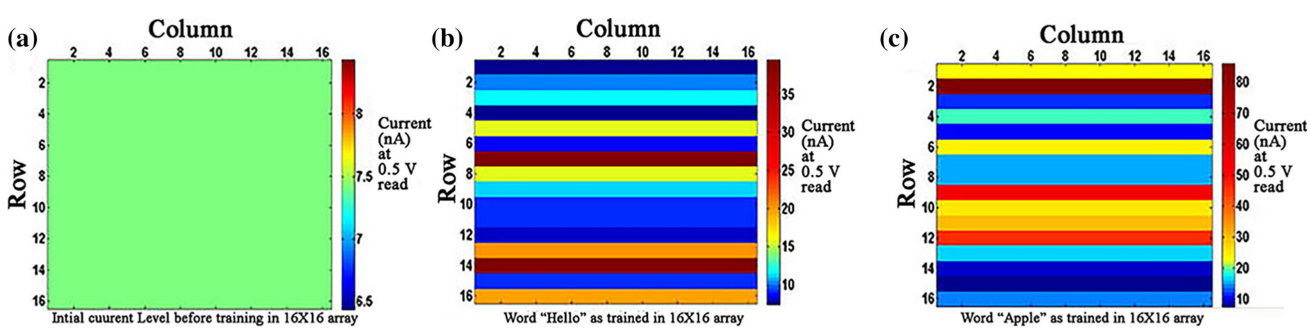


**Figure 10** Synaptic weights. **a** Initial current level. **b** The conductance distribution when the word "Hello" trained on the crossbar array of synaptic devices. **c**) The conductance distribution when the word "Apple" trained on the crossbar array of synaptic devices. Reprinted with permission from Ref. [3].

for real-time unsupervised spike sorting of complex brain signals. Synaptic weights are modulated through the application of an online learning strategy inspired by biological STDP. According to the report by Wang et al. [158] this network had been tested by real spiking data from the in vitro preparation of the crayfish sensory-motor system. The proposed RRAM was validated by different sets of real biological spiking data without parameter tuning (e.g., the threshold level for spike detection). This artificial SNN is able to identify, learn, recognize and distinguish between different spike shapes in the input signal with a recognition rate about 90% without any supervision.

$HfO_x$ is a superior RRAM material and the $HfO_x$-based synaptic device has demonstrated its application in neuromorphic computing, such as speech or pattern recognition. Gradual switching in the SET process can also be achieved through doping with trivalent metals, enabling the high-density applications.

## $TaO_x$-based synaptic devices

$TaO_x$-based synaptic devices have also attracted much attention. $TaO_x$ switching layer in an RRAM device usually consists of two phases: $TaO_2$ phase which is more conducting and $Ta_2O_5$ phase which is more insulating. The $TaO_x$ RRAM has been reported to possess high endurance ($> 10^{12}$ cycles), and its application in neuromorphic computing has been well demonstrated. $TaO_x$ could be engineered in synaptic device alone or combined with another oxide ($TiO_2$) layer in MIM structures. In this section, both single-layer $TaO_x$ or multi-layer $TaO_x$-based synaptic devices will be discussed.

Wang reported a high-density 3D synaptic architecture based on $Ta/TaO_x/TiO_2/Ti$ RRAM with ultralow sub-10 fJ energy per spike for neuromorphic computation in 2014 [159]. In addition, the analogue synaptic plasticity was simulated using the physical and compact models to facilitate future neuromorphic system designs. Thereafter, Wang et al. further investigated the synaptic device with the same structure experimentally and theoretically. The results showed that the device can be used for implementing concurrent inhibitory and excitatory synapses (Fig. 11). In addition, the devices also provided superior performances as compared to typical filamentary synaptic devices in reducing synaptic conductance and state fluctuation [160]. In the report, a physics-based compact model was also proposed for facilitating circuit-level design. Based on previous studies, the group successfully applied 3D two-layered $Ta/TaO_x/TiO_2/Ti$ cross-point synaptic array to implement highly anticipated hardware neural networks (HNN) in 2016 [161]. In total, more than 50 analogue synaptic weight states were controlled with minimal drifting during a cycling endurance test of 5000 training pulses. The team also proposed a new state-independent bipolar-pulse-training (BP) scheme, and this scheme significantly improved the nonlinearity of weight updates, consequently improving the training accuracy.

Similarly, $Ta/TaO_x/TiO_2/Ti$ synaptic devices were also reported by Gao et al. [162]. The device is forming-free, and more than 200 levels of conductance states could be continuously tuned by identical programming pulses. In addition, the team proposed a novel fully parallel write and read scheme to accelerate the weight update and increase energy efficiency in the training process on the chip. In order to engineer the conduction modulation linearity, Wang et al. [163] proposed a new approach in 2016 where a diffusion limiting layer ($SiO_2$) is inserted at the $TiN/TaO_x$ interface. The device exhibited higher switching linearity and lower power consumption that is desirable in neuromorphic computing hardware. Recently, $Pt/Ta_2O_{5-x}/W$ devices fabricated using vertical 3D architectures were demonstrated by Wang [164]. The proposed memory can be recovered with a timescale when the electrical stimulation was removed. This recoverable process can emulate the synaptic plasticity including rapid decay and slow decay stages of forgetting in the memory loss process of the human brain. Yao, P and his coworkers reported face classification using electronic synapses of $TaO_x/HfAl_yO_x$-based RRAM devices [165]. This optimized device structure has shown bidirectional continuous weight modulation behavior. A neuromorphic network is developed using analogue 1024-cell-1T1R RRAM array, and its application in grayscale face classification has been experimentally demonstrated with parallel online training. The energy consumption in each iteration is $1000 \times$ ($20 \times$) smaller than the Intel Xeon Phi processor with off-chip memory.

From our literature review, bilayer stack $TaO_x$/($HfAl_yO_x$, $TiO_x$) is intentionally designed as a synaptic device in the application of neuromorphic

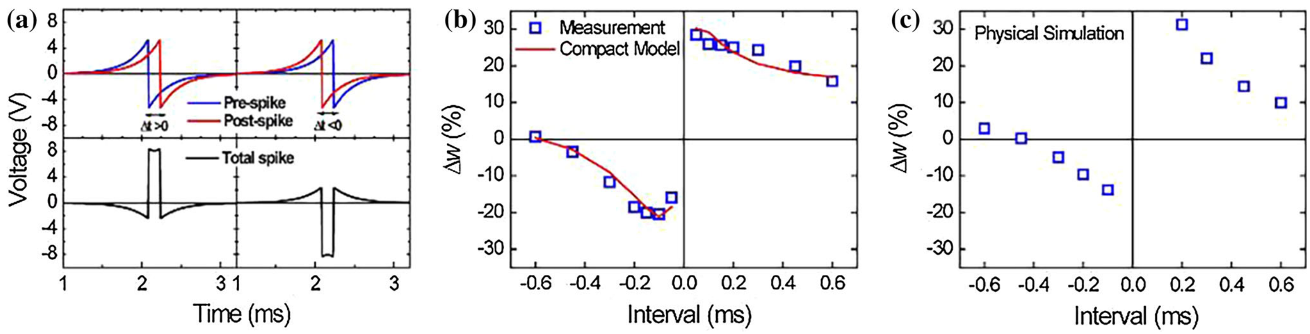


**Figure 11** Spike-timing-dependent plasticity (STDP). **a** Biomorphic-action-potential-like waveforms used for STDP measurement and simulation. The prespike pulse was applied to the Ta electrode, and the postspike pulse was applied to the Ti electrode. The potentiation and depression actions were controlled by the relative timing of the pre- and postspikes ($\Delta t$). The synapse weight change ($\Delta w$) was positive for $\Delta t > 0$, whereas it was negative for $\Delta t < 0$. **b** The measured $\Delta w$ as a function of $\Delta t$ for the Ta/$TaO_x$/$TiO_2$/Ti device. The red line shows the fitting result of using the physics-based compact model. **c** Simulation results for STDP, obtained by considering oxygen ion migration and the homogeneous barrier modulation model. Reprinted with permission from Ref [160].

computing. The possibility of engineering the $TaO_x$-based RRAM array in 3D structure enables the emulation of the high-density synaptic network in the real biological system.

## $TiO_x$-based synaptic devices

$TiO_x$ is one of earliest materials found to exhibit resistive switching property. In the previous section, $TaO_x$/$TiO_x$ bilayer structure RRAM for synaptic application has been introduced. Here, we will discuss other multi- and single-layer $TiO_x$-based synaptic devices.

In 2011, the synaptic performance of TiO was explored by Seo [46], demonstrating that $TiO_x$ and $TiO_y$ bilayer RRAMs exhibit analogue property where the multilevel conductance states were caused by the movement of oxygen ions between the two $TiO_x$ phase. The STDP was demonstrated by applying 100 successive identical pulses for potentiation or depression of synaptic weight. A year later, Yu developed $TiO_x$/$HfO_x$/$TiO_x$/$HfO_x$ multi-layer RRAM stacks exhibiting more gradual and smooth RESET switching for synaptic devices **[**166**].** Short pulses (10 ns) with an identical pulse amplitude enabled a sub-pJ energy per spike with potentially simple neuron circuits. Berdan emulated short-term synaptic dynamics with $TiO_2$ memristive devices in 2015 [167]. The meta-stable memory transitions in $TiO_2$ RRAM devices have proved to be the key feature to capture short-term synaptic dynamics. In addition to Seo, K works on bilayer $TiO_x$/$TiO_y$ RRAM structure in 2011 [46], Bousoulas, P studied amorphous–crystalline interfaces in $TiO_x$/$TiO_y$ RRAM structures for enhanced resistive switching and synaptic properties [168]. A physical model was also proposed to divulge the crucial role of temperature, electric potential and oxygen vacancy density on the switching effect. An 8 × 8 array of the neuron on a standard 6 M 180 nm of CMOS process as part of a larger multi-purpose neuromorphic chip was demonstrated by Mostafa, H as shown in Fig. 12 [169]. The proposed CMOS-memristor system comprises of CMOS neurons interconnected through $TiO_x$ memristors and spike-based learning circuits which modulate the conductance of the memristive synapse elements according to a spike-based perceptron plasticity rule. In 2016, Park developed a Mo/$TiO_x$-based interface RRAM and proposed a hybrid pulse mode for the synaptic application [170]. The $TiO_x$-based device is capable of producing 64-level conductance states, and the proposed hybrid pulse mode improves the symmetry of conductance change under both potentiation and depression conditions. The neural network simulation has shown that the hybrid pulse mode can enhance the pattern recognition accuracy of the proposed $TiO_x$ stack.

Although extensive investigations have been carried out on switching mechanism of $TiO_x$ RRAM, the demonstration of $TiO_x$ RRAM for neuromorphic computing is still limited when compared to the above-mentioned PCMO, $HfO_x$, $TaO_x$ materials. In most situations, $TiO_x$ is used in conjunction with bilayer or multi-layer synaptic device to optimize the performance.

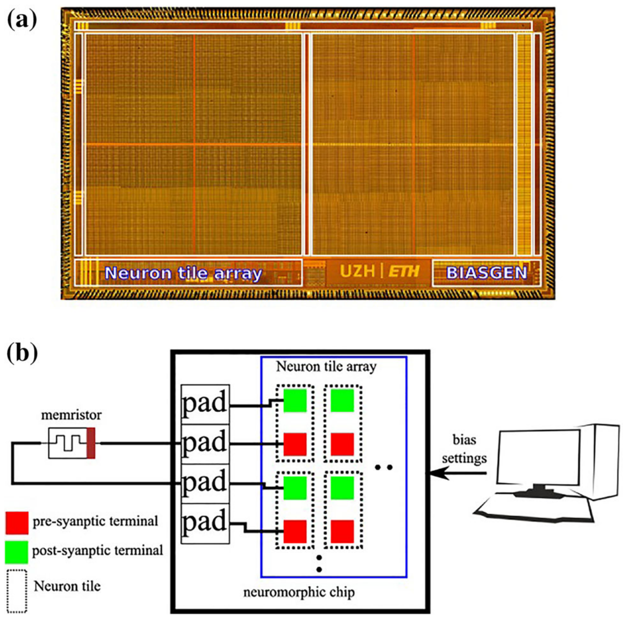


**Figure 12** **a** Micrograph of the multi-purpose neuromorphic chip die showing the neuron tile array and the bias generator. **b** Illustration of the hardware setup used to obtain measurements in this paper. The presynaptic terminal of one neuron tile is connected to the postsynaptic terminal of another neuron tile through an off-chip $TiO_{2-x}$ memristor. A PC controls the digital settings of the on-chip bias generator. Reprinted with permission from Ref. [169].

## $NiO_x$-based synaptic devices

Similar to $TiO_x$, $NiO_x$ is one of earliest materials found to exhibit restive switching behavior. Although $NiO_x$-based RRAM devices have been reported with high endurance ($10^6$) and retention, its application for neuromorphic computing is restricted due to the poor uniformity. A bipolar $NiO_x$ RRAM, two NMOS FET and a capacitor were used to fabricate analogue synaptic devices (circuits) by Akoh [171]. This device also has the ability to update the synaptic conductance according to the difference of pre- and post-neuron spike timing. In 2013, Hu emulated the paired-pulse facilitation of biological synapse with $NiO_x$-based memristor, thus creating a form of short-term synaptic plasticity [172]. It was also observed that the current in $NiO_x$-based memristor had increased after a second electrical pulse. Additionally, the magnitude of the facilitation decreases with the pulse interval and it increases with the pulse magnitude or pulse width. Hu, S.G and his coworkers realized the well-known Pavlov's dog model with $NiO_x$-based memristor [173]. The long-term potentiation behavior was emulated by the increase in memristor's conductance when applying the electrical pulses. In addition, spontaneous conductance decaying toward its initial state resembles the synaptic long-term potentiation. Finally, an artificial neural network was constructed to realize the Pavlov's dog model (Fig. 13).

## $WO_x$-based synaptic devices

Tungsten oxides ($WO_x$) are another great candidate for memristive devices as a bio-inspired artificial synapse. The advantage of $WO_x$-based synaptic devices includes accredited endurance ($10^5$ cycles), CMOS compatibility and memorization and learning functions. Here, we highlight the implementation of this material in neuromorphic computing as a biological artificial synapse.

Synaptic behaviors and modeling of a $WO_x$ memristive device were reported by Chang [174] .The Pd/$WO_x$/W-structured memristor device shows reliable synaptic operations with good endurance. The synaptic devices can endure at least $10^5$ potentiation/depression pulses without degradation. Furthermore, the memristor behavior was explained by a novel model that takes both drift and diffusion effects into consideration. Figure 14 presents the retention loss

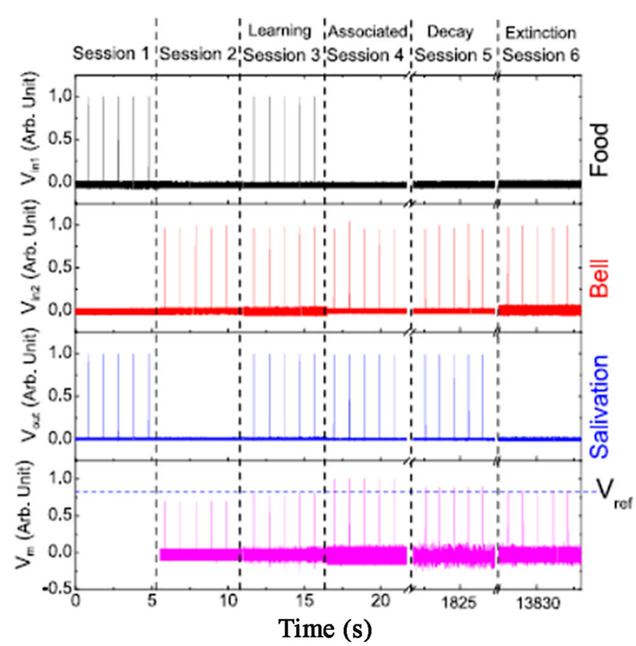


**Figure 13** Learning and forgetting of association in Pavlov's dog experiment realized with the three-neuron neural network. Reprinted with permission from Ref [173].

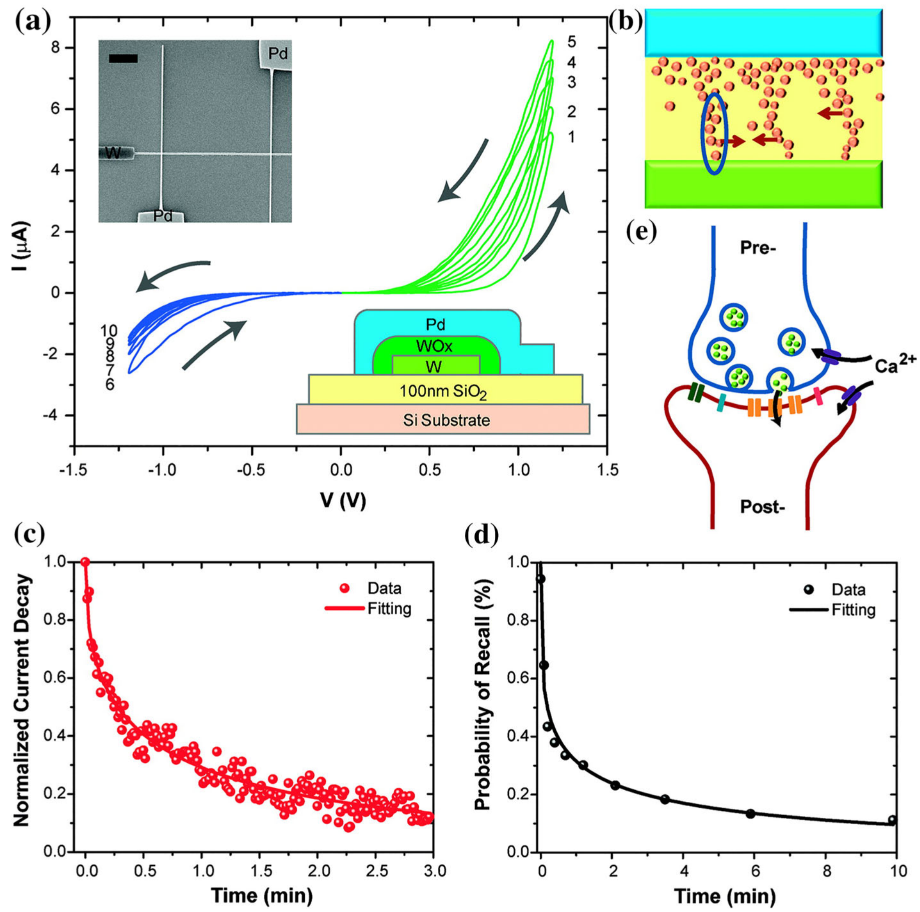


**Figure 14** **a** DC *I–V* curves of a memristor studied. **b** Schematic illustration of oxygen vacancy diffusion. **c** Retention loss curve of Pd/$WO_x$/W-based memristor. **d** Forgetting memory of human memory curve. **e** Schematic illustration of synaptic plasticity modulation. Reprinted with permission from Ref [47].

curve and forgetting memory in a human memory curve from a paper by Chang [47]. It was found that the trend of retention curve of a Pd/$WO_x$/W-based memristor and human forgetting curves greatly correspond to each other and both can be fitted using a stretched-exponential function (SEF). In addition, the temperature and humidity impact on the performance of a $WO_x$ memristive device was studied by Meng et al. and Yong et al., respectively [175, 176]. According to the simulation results, the synaptic weight of $WO_x$ memristive device decays faster as the temperature increases due to higher oxygen vacancies diffusion. In addition to the temperature, the memristive effects of tungsten oxide are also highly humidity dependent. The adsorbed moisture on the surface of $WO_3$ has resulted in decreasing conductances as the H cation induces an increase in barrier heights.

Among other transition metal oxides, $WO_x$ is a great candidate material for synaptic devices application. For further exploring its application in neuromorphic computing, enhancement of synaptic operation time (endurance) is of importance.

## $AlO_x$-based synaptic devices

The resistive switching behavior in $AlO_x$ was first reported by Hickmott [1]. $AlO_x$ is of interest in RRAM materials due to its large band gap ($\sim$ 9 eV) and low RESET current ($\sim$ μA). For neuromorphic application, $AlO_x$ can also be used alone or stacked with other RRAM materials to improve the uniformity of the synaptic device characteristics.

$AlO_x$-based resistive switching device was investigated by Wu [49] to serve as a potential electronic synapse device. The 0.48 μm × 0.48 μm Ti/$AlO_x$/TiN memory stack exhibited multi-level resistance states when varying the compliance current levels or the applied voltage amplitudes during pulse cycling. In his work, around 1% resistance change per pulse cycling was obtained and an STDP realization scheme was proposed to implement the synaptic device in large-scale hardware neuromorphic computing system. In 2015, Prezioso experimentally characterized $Al_2O_3/TiO_2$-based memristors to modulate the impact of conductance-dependent conductance change on short-term dependent plasticity [177]. The utilization of $TiO_x/Al_2O_3$-based memristor devices to emulate biological synaptic behavior for building brain-inspired computers was explored by Banerjee, W.et al. in 2017 [178]. The proposed $TiO_2/Al_2O_3$ synaptic device has the capability to switch from short-term memory (STM) to long-term memory (LTM) by introducing a mezzanine state at medium memory (MM) as shown in Fig. 15. In the paper, the dependence of retention (decay time) on conductance levels (memory level) was investigated and an experimentally proven psychological model is presented.

Till now, the potential validity of $Al_2O_3$ materials for electronic synapses had been experimentally demonstrated. Nevertheless, the reports of sophisticated $Al_2O_3$-based memristor as an artificial synapse are limited. Therefore, further verification with different structures is required.

## Other oxide-based synaptic devices

Besides the materials discussed above, a variety of other materials has been studied to implement neural network as a synaptic device. $FeO_x$-based RRAM with mixed-analogue–digital behavior was investigated by Deng et al. [12] for a recurrent neural network using the recursive least-squares algorithm.

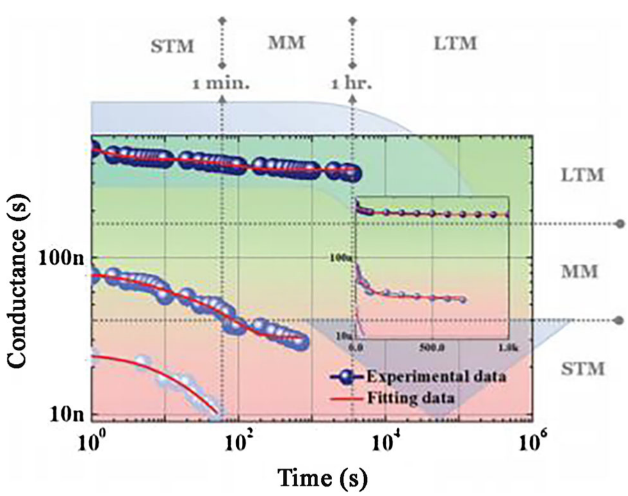


**Figure 15** Memory effects in the TiOx/$Al_2O_3$-based electronic synaptic junction. The figure shows the conductance failure with time. A linear scale plot is shown in the inset of the figure. Reprinted with permission from Ref [178].

Wang, C.H et al. reported the synaptic behavior of a $FeO_x$-based RRAM in which the dependence of compliance current on conductance stability was studied [179]. The application of $CeO_2$-based RRAM for highly energy efficient neuromorphic systems was demonstrated by Kim et al. The $Pt/CeO_2/Pt$ device exhibited the polarity-dependent and asymmetric diode-type resistive switching [180], and the detailed switching characteristics of artificial synapses (potentiation and depression) were discussed. A $GdO_x$ and Cu-doped $MoO_x$ stack with a platinum top and bottom electrodes were reported by Choi [45]. The weighted sum operation was carried out on electrically modifiable synapse array circuit based on the proposed stacks [181]. The biological synaptic behavior was demonstrated by Chang through integrating $SiO_x$-based RRAM with Si diodes. The proposed one-diode-one-resistor (1D-1R) architecture not only avoids sneak-path issues and lowers standby power consumption, but also helps to realize STDP behaviors [182]. $VO_x$ is a well-known Mott material which experience sharp and first-order metal-to-insulator transition (MIT) at the around 68 °C [183]. The application of $VO_x$ as RRAM materials had been explored by Drisoll et al. [184] through sol–gel technique. Nevertheless, most researches on $VO_x$ so far focus on its use for select device which can be integrated with RRAM device to mitigate sneak-path current. The $Pt/VO_2/Pt$ selector has been integrated with NiO unipolar RRAM by Lee et al. [185] in 2007 and $ZrO_x/HfO_x$ bipolar RRAM by Son et al. [186] in 2011. In 2016, 1S1R configuration of $W/VO_2/Pt$ selection device and $Ti/HfO_2/Pt$ RRAM was demonstrated by Kailiang et al. [187]. However, thermal instability is a major challenge for $VO_2$ for practical applications [14].

## Summary and outlook

In conclusion, we have outlined an overview of oxide-based RRAM materials for the applications in neuromorphic computing. Table 5 summarizes the RRAM materials and their parameters discussed in this review. Our work suggested that the neuromorphic approach with oxide-based RRAM devices is promising. So far, PCMO, $HfO_x$, $TaO_x$, $TiO_x$, $NiO_x$, $WO_x$, $AlO_x$, etc., materials have been demonstrated for their application in oxide-based synaptic devices. However, challenges still remain in specific materials,

**Table 5** Summary of RRAM materials in this review

| Material | On/off ratio | Endurance | Energy consumption | Multi-levels | Switching time | Neuromorphic computing applications |
|---|---|---|---|---|---|---|
| PCMO [97, 136–146] | $10^3$ | $10^5$ | 6 pJ | 32 | 8 ns | Pattern recognition<br>Human thought patterns<br>Neural fear-conditioning signal recognition |
| $HfO_x$ [147–151] | $10^2$ | $10^6$ | 10 pJ | 8 | 10 ns | Speech recognition<br>Visual pattern recognition |
| $TaO_x$ [158–164] | 10X | $10^{12}$ | 10 fJ | 200 | 105 ps | Grayscale face classification |
| $TiO_x$ [46, 166–170, 189] | $10^5$ | 2 X $10^6$ | sub-pJ | 64 | 5 ns | Pattern recognition in simulation |
| $NiO_x$ [171–173, 185, 190, 191] | $10^6$ | $10^6$ | – | 5 | 20 ns | Learning and forgetting of association in Pavlov's dog experiment realized. |
| $WO_x$ [47, 174–176, 192] | $10^3$ | $10^5$ | – | 8 | 50 ns | Human forgetting curves |
| $AlO_x$ [49, 193–195] | $10^6$ | $10^5$ | 1.5 pJ | 10 | 10 ns | Spike-timing-dependent plasticity realization scheme. |
| $FeO_x$ [179, 196, 197] | $10^2$ | $6 \times 10^4$ | – | 6 | 10 ns | Long-term potentiation and long-term depression demonstration |
| $CeO_2$ [180, 198] | $10^5$ | $10^4$ | – | 8 | 200 ns | Synaptic potentiation and depression characteristics demonstration |
| $MoO_x$ [39, 199] | 10× | $10^6$ | – | 8 | 1 ms | Weighted sum operation carried out on MoOx-based electrically modifiable synapse array circuit |
| $SiO_x$ [182, 200–202] | $10^7$ | $10^6$ | – | 4 | 100 ps | Long-term potentiation and long-term depression demonstration |

e.g., poor symmetric weight update for $PCMO_x$-based synaptic devices and low endurance for $WO_x$-based synaptic devices. In general, there are two main key challenges for overall oxide-based RRAM materials. Although the inherent fault tolerance of neural network models is able to mitigate the impact of device variation to some extent, the improvement of spatial variation and temporal variation turns out to be one of the greatest challenges on a long-term basis. In addition, improvement of reliability characteristics of the RRAM synaptic devices is another key challenge which is not well studied.

In future material research of neuromorphic computing applications, the study of novel tunable materials with enhanced properties for neuromorphic devices is one of the most exciting components. One such example is MgO, which has a large band gap that ensures sufficient band offsets, a high dielectric constant that might potentially reduce leakage current (thus improving device scalability), a high thermal conductivity which minimizes self-heating during operations and a large breakdown field that might prevent the device from irreversible damages. In addition, MgO-based magnetic tunnel junction memristors had been proposed for implementation of synapses [188]. Further research is required to expand the database of materials for synaptic devices and neuromorphic applications.

Finally, to implement oxide-based RRAM devices as a synapse in neuromorphic systems, it is imperative to have an in-depth understanding of the metaplasticity mechanism and internal states of these memristive devices. The underlying mechanisms governing RRAM devices will inevitably be discovered from investigations of conduction and resistive switching mechanism via results from either experiment or simulation. Further research work incorporating interactions between materials, device levels, circuit designs and computing processes will certainly speed up the realization of oxide-based RRAM synapses for neuromorphic systems.

## Acknowledgements

This work was supported by a RIE2020 AME-Programmatic Grant (Neuromorphic computing, No. A1687b0033) and an Industry-IHL Partnership Program (NRF2015-IIP001-001). WSL is a member of the Singapore Spintronics Consortium (SG-SPIN).

## References

[1] Hickmott TW (1962) Low-frequency negative resistance in thin anodic oxide films. J Appl Phys 33(9):2669–2682. https://doi.org/10.1063/1.1702530

[2] Liu SQ, Wu NJ, Ignatiev A (2000) Electric-pulse-induced reversible resistance change effect in magnetoresistive films. Appl Phys Lett 76(19):2749–2751. https://doi.org/10.1063/1.126464

[3] Mandal S, El-Amin A, Alexander K, Rajendran B, Jha R (2014) Novel synaptic memory device for neuromorphic computing. Sci Rep. https://doi.org/10.1038/srep05333

[4] Lee MJ, Park Y, Kang BS, Ahn SE, Lee C, Kim K, Xianyu WX, Stefanovich G, Lee JH, Chung SJ, Kim YH, Lee CS, Park JB, Baek IG, Yoo IK (2007) 2-Stack 1D-1R cross-point structure with oxide diodes as switch elements for high density resistance RAM applications. In: International electron devices meeting, 2007, pp 771–774. https://doi.org/10.1109/iedm.2007.4419061

[5] Strukov DB, Snider GS, Stewart DR, Williams RS (2008) The missing memristor found. Nature 453(7191):80–83. https://doi.org/10.1038/nature06932

[6] Chevallier CJ, Siau CH, Lim SF, Namala SR, Matsuoka M, Bateman BL, Rinerson D (2010) A 0.13 μm 64 Mb multi-layered conductive metal-oxide memory. In: 2010 IEEE international solid-state circuits conference—(ISSCC), pp 260–261

[7] Liu TY, Yan TH, Scheuerlein R, Chen YC, Lee JK, Balakrishnan G, Yee G, Zhang H, Yap A, Ouyang JW, Sasaki T, Al-Shamma A, Chen CY, Gupta M, Hilton G, Kathuria A, Lai V, Matsumoto M, Nigam A, Pai A, Pakhale J, Siau CH, Wu XX, Yin YB, Nagel N, Tanaka Y, Higashitani M, Minvielle T, Gorla C, Tsukamoto T, Yamaguchi T, Okajima M, Okamura T, Takase S, Inoue H, Fasoli L (2014) A 130.7-mm(2) 2-layer 32-Gb ReRAM memory device in 24-nm technology. IEEE J Solid-State Circuits 49(1):140–153

[8] Fackenthal R, Kitagawa M, Otsuka W, Prall K, Mills D, Tsutsui K, Javanifard J, Tedrow K, Tsushima T, Shibahara Y, Hush G (2014) A 16 Gb ReRAM with 200 MB/s write and 1 GB/s read in 27 nm technology. In: ISSCC digest technical papers IEEE international, vol 57, pp 338–339

[9] Luo Q, Xu X, Liu H, Lv H, Gong T, Long S, Liu Q, Sun H, Banerjee W, Li L, Gao J, Lu N, Liu M (2016) Super non-linear RRAM with ultra-low power for 3D vertical nano-crossbar arrays. Nanoscale 8(34):15629–15636. https://doi.org/10.1039/C6NR02029A

[10] Mertens R (2017) Digitimes. http://www.digitimes.com/newregister/join.asp?view=Article&DATEPUBLISH=2017/06/05&PAGES=PB&SEQ=200. June 08, 2017

[11] Chang T-C, Chang K-C, Tsai T-M, Chu T-J, Sze SM (2016) Resistance random access memory. Mater Today 19(5):254–264. https://doi.org/10.1016/j.mattod.2015.11.009

[12] Deng L, Li G, Deng N, Wang D, Zhang Z, He W, Li H, Pei J, Shi L (2015) Complex learning in bio-plausible memristive networks. Sci Rep 5:10684. https://doi.org/10.1038/srep10684

[13] Advances and Trends of RRAM technology SemiconTaiwan (2015)

[14] Wong HSP, Lee HY, Yu SM, Chen YS, Wu Y, Chen PS, Lee B, Chen FT, Tsai MJ (2012) Metal-oxide RRAM. Proc IEEE 100(6):1951–1970. https://doi.org/10.1109/Jproc.2012.2190369

[15] Kuzum D, Yu SM, Wong HSP (2013) Synaptic electronics: materials, devices and applications. Nanotechnology. https://doi.org/10.1088/0957-4484/24/38/382001

[16] Akinaga H, Shima H (2010) Resistive random access memory (ReRAM) based on metal oxides. Proc IEEE 98(12):2237–2251. https://doi.org/10.1109/Jproc.2010.2070830

[17] Waser R, Aono M (2007) Nanoionics-based resistive switching memories. Nat Mater 6(11):833–840. https://doi.org/10.1038/nmat2023

[18] Chi P, Li SC, Xu C, Zhang T, Zhao JS, Liu YP, Wang Y, Xie Y (2016) PRIME: a novel processing-in-memory architecture for neural network computation in ReRAM-based main memory. In: Conference proceedings of international symposium coastal engineering, pp 27–39. https://doi.org/10.1109/isca.2016.13

[19] Qian K, Nguyen VC, Chen TP, Lee PS (2016) Novel concepts in functional resistive switching memories. J Mater Chem C 4(41):9637–9645. https://doi.org/10.1039/c6tc03447k

[20] Tsunoda K, Kinoshita K, Noshiro H, Yamazaki Y, Iizuka T, Ito Y, Takahashi A, Okano A, Sato Y, Fukano T, Aoki M, Sugiyama Y (2007) Low power and high speed switching

of Ti-doped NiOReRAM under the unipolar voltage source of less than 3 V. In: International electron devices meeting, pp 767–770. https://doi.org/10.1109/iedm.2007.4419060

[21] Wang ZR, Zhu WG, Du AY, Wu L, Fang Z, Tran XA, Liu WJ, Zhang KL, Yu HY (2012) Highly uniform, self-compliance, and forming-free ALD HfO2-based RRAM with Ge doping. IEEE Trans Electron Dev 59(4):1203–1208. https://doi.org/10.1109/Ted.2012.2182770

[22] Magyari-Kope B, Duncan D, Zhao L, Nishi Y (2016) Doping technology for RRAM—opportunities and challenges. In: International symposium on VLSI technology

[23] Yu S, Wu Y, Chai Y, Provine J, Wong HSP (2011) Characterization of switching parameters and multilevel capability in HfOx/AlOx bi-layer RRAM devices. In: VLSI technology (VLSIT), 2011 symposium on, pp 106–107

[24] Park SG, Yang MK, Ju H, Seong DJ, Lee JM, Kim E, Jung S, Zhang L, Shin YC, Baek IG, Choi J, Kang HK, Chung C (2012) A non-linear ReRAM cell with sub-1 mu a ultralow operating current for high density vertical resistive memory (VRRAM). In: 2012 IEEE international electron devices meeting (IEDM)

[25] Yun JB, Kim S, Seo S, Lee MJ, Kim DC, Ahn SE, Park Y, Kim J, Shin H (2007) Random and localized resistive switching observation in Pt/NiO/Pt. Phys Status Solidi-R 1(6):280–282. https://doi.org/10.1002/pssr.200701205

[26] Ho PWC, Hatem FO, Almurib HAF, Kumar TN (2016) Comparison between Pt/TiO2/Pt and Pt/TaOX/TaOY/Pt based bipolar resistive switching devices. J Semicond. https://doi.org/10.1088/1674-4926/37/6/064001

[27] Lei XY, Liu HX, Gao HX, Yang HN, Wang GM, Long SB, Ma XH, Liu M (2014) Resistive switching characteristics of Ti/ZrO2/Pt RRAM device. Chin Phys B. https://doi.org/10.1088/1674-1056/23/11/117305

[28] Long SB, Lian XJ, Ye TC, Cagli C, Perniola L, Miranda E, Liu M, Sune J (2013) Cycle-to-cycle intrinsic RESET statistics in HfO2-based unipolar RRAM devices. IEEE Electron Dev Lett 34(5):623–625. https://doi.org/10.1109/Led.2013.2251314

[29] Yoshida C, Tsunoda K, Noshiro H, Sugiyama Y (2007) High speed resistive switching in Pt/TiO2/TiN film for nonvolatile memory application. Appl Phys Lett. https://doi.org/10.1063/1.2818691

[30] Xu N, Liu LF, Sun X, Chen C, Wang Y, Han DD, Liu XY, Han RQ, Kang JF, Yu B (2008) Bipolar switching behavior in TiN/ZnO/Pt resistive nonvolatile memory with fast switching and long retention. Semicond Sci Technol. https://doi.org/10.1088/0268-1242/23/7/075019

[31] Kim S, Lee D, Park J, Jung S, Lee W, Shin J, Woo J, Choi G, Hwang H (2012) Defect engineering: reduction effect of hydrogen atom impurities in HfO2-based resistive-switching memory devices. Nanotechnology. https://doi.org/10.1088/0957-4484/23/32/325702

[32] Ma G, Tang X, Zhang H, Zhong Z, Li X, Li J, Su H (2017) Ultra-high ON/OFF ratio and multi-storage on NiO resistive switching device. J Mater Sci 52(1):238–246. https://doi.org/10.1007/s10853-016-0326-5

[33] Sarkar PK, Prajapat M, Barman A, Bhattacharjee S, Roy A (2016) Multilevel resistance state of Cu/La2O3/Pt forming-free switching devices. J Mater Sci 51(9):4411–4418. https://doi.org/10.1007/s10853-016-9753-6

[34] Tsai CL, Xiong F, Pop E, Shim M (2013) Resistive random access memory enabled by carbon nanotube crossbar electrodes. ACS Nano 7(6):5360–5366. https://doi.org/10.1021/nn401212p

[35] Wu Y, Chai Y, Chen H-Y, Yu S, Wong H-SP (2011) Resistive switching AlOx-based memory with CNT electrode for ultra-low switching current and high density memory application. In: VLSI technology (VLSIT), 2011 Symposium on

[36] Munoz-Gorriz J, Acero MC, Gonzalez MB, Campabadal F (2017) Top electrode dependence of the resistive switching behavior in HfO2/n(+)Si-based devices. In: Spanish conference electron

[37] Sohn J, Lee S, Jiang ZZ, Chen HY, Wong HSP (2014) Atomically thin graphene plane electrode for 3D RRAM. In: 2014 IEEE international electron devices meeting (IEDM)

[38] Cheng CH, Chin A, Yeh FS (2011) Ultralow switching energy Ni/GeOx/HfON/TaN RRAM. IEEE Electron Device Lett 32(3):366–368. https://doi.org/10.1109/Led.2010.2095820

[39] Yoon J, Choi H, Lee D, Park JB, Lee J, Seong DJ, Ju Y, Chang M, Jung S, Hwang H (2009) Excellent switching uniformity of Cu-Doped MoOx/GdOx bilayer for nonvolatile memory applications. IEEE Electron Device Lett 30(5):457–459. https://doi.org/10.1109/Led.2009.2015687

[40] Yu SM, Gao B, Fang Z, Yu HY, Kang JF, Wong HSP (2013) A low energy oxide-based electronic synaptic device for neuromorphic visual systems with tolerance to device variation. Adv Mater 25(12):1774–1779. https://doi.org/10.1002/adma.201203680

[41] Lee AR, Bae YC, Baek GH, Im HS, Hong JP (2013) Multilevel resistive switching observations in asymmetric Pt/Ta2O5 − x/TiOxNy/TiN/Ta2O5 − x/Pt multilayer configurations. Appl Phys Lett. https://doi.org/10.1063/1.4818129

[42] Kumar D, Aluguri R, Chand U, Tseng TY (2017) Metal oxide resistive switching memory: materials, properties and switching mechanisms. Ceram Int 43:S547–S556. https://doi.org/10.1016/j.ceramint.2017.05.289

[43] Drachman DA (2005) Do we have brain to spare? Neurology 64(12):2004–2005. https://doi.org/10.1212/01.Wnl.0000166914.38327.Bb
[44] Suri M, Bichler O, Querlioz D, Palma G, Vianello E, Vuillaume D, Gamrat C, DeSalvo B (2012) CBRAM devices as binary synapses for low-power stochastic neuromorphic systems: auditory (Cochlea) and visual (Retina) cognitive processing applications. In: 2012 IEEE international electron devices meeting (IEDM)
[45] Choi H, Jung H, Lee J, Yoon J, Park J, Seong DJ, Lee W, Hasan M, Jung GY, Hwang H (2009) An electrically modifiable synapse array of resistive switching memory. Nanotechnology. https://doi.org/10.1088/0957-4484/20/34/345201
[46] Seo K, Kim I, Jung S, Jo M, Park S, Park J, Shin J, Biju KP, Kong J, Lee K, Lee B, Hwang H (2011) Analog memory and spike-timing-dependent plasticity characteristics of a nanoscale titanium oxide bilayer resistive switching device. Nanotechnology. https://doi.org/10.1088/0957-4484/22/25/254023
[47] Chang T, Jo SH, Lu W (2011) Short-term memory to long-term memory transition in a nanoscale memristor. ACS Nano 5(9):7669–7676. https://doi.org/10.1021/nn202983n
[48] Yang R, Terabe K, Liu GQ, Tsuruoka T, Hasegawa T, Gimzewski JK, Aono M (2012) On-demand nanodevice with electrical and neuromorphic multifunction realized by local ion migration. ACS Nano 6(11):9515–9521. https://doi.org/10.1021/nn302510e
[49] Wu Y, Yu SM, Wong HSP, Chen YS, Lee HY, Wang SM, Gu PY, Chen F, Tsai MJ (2012) AlOx-based resistive switching device with gradual resistance modulation for neuromorphic device application. In: IEEE international memory workshop
[50] Suri M, Bichler O, Hubert Q, Perniola L, Sousa V, Jahan C, Vuillaume D, Gamrat C, DeSalvo B (2012) Interface engineering of PCM for improved synaptic performance in neuromorphic systems. In: IEEE international memory workshop
[51] Eryilmaz SB, Kuzum D, Jeyasingh R, Kim S, BrightSky M, Lam C, Wong HSP (2014) Brain-like associative learning using a nanoscale non-volatile phase change synaptic device array. Front Neurosci-Switz. https://doi.org/10.3389/fnins.2014.00205
[52] Garbin D, Suri M, Bichler O, Querlioz D, Gamrat C, DeSalvo B (2013) Probabilistic neuromorphic system using binary phase-change memory (PCM) synapses: detailed power consumption analysis. In: 2013 13th IEEE conference on nanotechnology (IEEE-Nano), pp 91–94
[53] Jo SH, Chang T, Ebong I, Bhadviya BB, Mazumder P, Lu W (2010) Nanoscale memristor device as synapse in neuromorphic systems. Nano Lett 10(4):1297–1301. https://doi.org/10.1021/nl904092h
[54] Kang DH, Jun HG, Ryoo KC, Jeong H, Sohn H (2015) Emulation of spike-timing dependent plasticity in nano-scale phase change memory. Neurocomputing 155:153–158. https://doi.org/10.1016/j.neucom.2014.12.036
[55] Kim S, Ishii M, Lewis S, Perri T, BrightSky M, Kim W, Jordan R, Burr GW, Sosa N, Ray A, Han JP, Miller C, Hosokawa K, Lam C (2015) NVM neuromorphic core with 64 k-cell (256-by-256) phase change memory synaptic array with on-chip neuron circuits for continuous in situ learning. In: 2015 IEEE international electron devices meeting (IEDM)
[56] Shelby RM, Burr GW, Boybat I, Di Nolfo C (2015) Non-volatile memory as hardware synapse in neuromorphic computing: a first look at reliability issues. In: 2015 IEEE international reliability physics symposium (IRPS)
[57] Suri M, Bichler O, Querlioz D, Cueto O, Perniola L, Sousa V, Vuillaume D, Gamrat C, DeSalvo B (2011) Phase change memory as synapse for ultra-dense neuromorphic systems: application to complex visual pattern extraction. In: 2011 IEEE international electron devices meeting (IEDM)
[58] Suri M, Bichler O, Querlioz D, Traore B, Cueto O, Perniola L, Sousa V, Vuillaume D, Gamrat C, DeSalvo B (2012) Physical aspects of low power synapses based on phase change memory devices. J Appl Phys. https://doi.org/10.1063/1.4749411
[59] Zhong YP, Li Y, Xu L, Miao XS (2015) Simple square pulses for implementing spike-timing-dependent plasticity in phase-change memory. Phys Status Solidi-R 9(7):414–419. https://doi.org/10.1002/pssr.201510150
[60] Kuzum D, Jeyasingh RGD, Lee B, Wong HSP (2012) Nanoelectronic programmable synapses based on phase change materials for brain-inspired computing. Nano Lett 12(5):2179–2186. https://doi.org/10.1021/nl201040y
[61] Kuzum D, Jeyasingh RGD, Wong HSP (2011) Energy efficient programming of nanoelectronic synaptic devices for large-scale implementation of associative and temporal sequence learning. In: 2011 IEEE international electron devices meeting (IEDM)
[62] Sharad M, Augustine C, Roy K (2012) Boolean and non-boolean computation with spin devices. In: 2012 IEEE international electron devices meeting (IEDM)
[63] Sangwan VK, Jariwala D, Kim IS, Chen KS, Marks TJ, Lauhon LJ, Hersam MC (2015) Gate-tunable memristive phenomena mediated by grain boundaries in single-layer MoS2. Nat Nanotechnol 10(5):403–406. https://doi.org/10.1038/Nnano.2015.56

[64] Sengupta A, Al Azim Z, Fong XY, Roy K (2015) Spin-orbit torque induced spike-timing dependent plasticity. Appl Phys Lett. https://doi.org/10.1063/1.4914111

[65] Sengupta A, Parsa M, Han B, Roy K (2016) Probabilistic deep spiking neural systems enabled by magnetic tunnel junction. IEEE Trans Electron Dev 63(7):2963–2970. https://doi.org/10.1109/Ted.2016.2568762

[66] Sengupta A, Roy K (2016) Short-term plasticity and long-term potentiation in magnetic tunnel junctions: towards volatile synapses. Phys Rev Appl. https://doi.org/10.1103/PhysRevApplied.5.024012

[67] Adachi M, Seki M, Yamahara H, Nasu H, Tabata H (2015) Long-term potentiation of magnonic synapses by photo-controlled spin current mimicked in reentrant spin-glass garnet ferrite Lu3Fe5-2xCoxSixO12 thin films. Appl Phys Express. https://doi.org/10.7567/Apex.8.043002

[68] Roska T, Horvath A, Stubendek A, Corinto F, Csaba G, Porod W, Shibata T, Bourianoff G (2012) An associative memory with oscillatory CNN arrays using spin torque oscillator cells and spin-wave interactions architecture and end-to-end simulator. In: International work cell nano

[69] Fujita O, Amemiya Y (1993) A floating-gate analog memory device for neural networks. IEEE Trans Electron Dev 40(11):2029–2055. https://doi.org/10.1109/16.239745

[70] Hafliger P, Rasche C (1999) Floating gate analog memory for parameter and variable storage in a learning silicon neuron. In: ISCAS '99: proceedings of the 1999 IEEE international symposium on circuits and systems, vol 2, pp 416–419

[71] Harrison RR, Bragg JA, Hasler P, Minch BA, Deweerth SP (2001) A CMOS programmable analog memory-cell array using floating-gate circuits. IEEE Trans Circuits-II 48(1):4–11. https://doi.org/10.1109/82.913181

[72] Brink S, Nease S, Hasler P (2013) Computing with networks of spiking neurons on a biophysically motivated floating-gate based neuromorphic integrated circuit. Neural Netw 45:39–49. https://doi.org/10.1016/j.neunet.2013.02.011

[73] Diorio C, Hasler P, Minch BA, Mead CA (1997) A floating-gate MOS learning array with locally computed weight updates. IEEE Trans Electron Dev 44(12):2281–2289. https://doi.org/10.1109/16.644652

[74] Diorio C, Hasler P, Minch BA, Mead C (1997) A complementary pair of four-terminal silicon synapses. Analog Integr Circ Signal Process 13(1–2):153–166. https://doi.org/10.1023/A:1008244314595

[75] Rahimi K, Diorio C, Hernandez C, Brockhausen MD (2002) A simulation model for floating-gate MOS synapse transistors. In: 2002 IEEE international symposium on circuits and systems, vol II, proceedings, pp 532–535

[76] Diorio C, Hasler P, Minch A, Mead CA (1996) A single-transistor silicon synapse. IEEE Trans Electron Dev 43(11):1972–1980. https://doi.org/10.1109/16.543035

[77] Cauwenberghs G, Neugebauer CF, Agranat AJ, Yariv A (1990) Large scale optoelectronic integration of asynchronous analog neural networks. In: International neural network conference: July 9–13, 1990 Palais Des Congres—Paris—France. Springer, Netherlands, pp 551–554. https://doi.org/10.1007/978-94-009-0643-3_1

[78] Burla M, Wang X, Li M, Chrostowski L, Azana J (2016) Wideband dynamic microwave frequency identification system using a low-power ultracompact silicon photonic chip. Nat Commun. https://doi.org/10.1038/ncomms13004

[79] Rietman EA, Frye RC, Wong CC, Kornfeld CD (1989) Amorphous-silicon photoconductive arrays for artificial neural networks. Appl Opt 28(16):3474–3478

[80] Livingston DL, Albin S, Park SM (1991) A new method for storing weights in analog neural hardware. In: IEEE proceedings of the Southeastcon 91, vols 1 and 2, pp 86–88. https://doi.org/10.1109/secon.1991.147710

[81] Maier P, Hartmann F, Emmerling M, Schneider C, Kamp M, Hofling S, Worschech L (2016) Electro-photo-sensitive memristor for neuromorphic and arithmetic computing. Phys Rev Appl. https://doi.org/10.1103/PhysRevApplied.5.054011

[82] Boukhobza J, Rubini S (2012) Flashing in the memory hierarchy: an overview on flash memory internals

[83] Kotecki DE (1997) A review of high dielectric materials for DRAM capacitors. Integr Ferroelectr 16(1–4):1–19. https://doi.org/10.1080/10584589708013025

[84] Pavan P, Bez R, Olivo P, Zanoni E (1997) Flash memory cells: an overview. Proc IEEE 85(8):1248–1271. https://doi.org/10.1109/5.622505

[85] Sethi P, Krishnia S, Gan WL, Kholid FN, Tan FN, Maddu R, Lew WS (2017) Bi-directional high speed domain wall motion in perpendicular magnetic anisotropy Co/Pt double stack structures. Sci Rep. https://doi.org/10.1038/s41598-017-05409-7

[86] Zhang SF, Gan WL, Kwon J, Luo FL, Lim GJ, Wang JB, Lew WS (2016) Highly efficient domain walls injection in perpendicular magnetic anisotropy nanowire. Sci Rep. https://doi.org/10.1038/srep24804

[87] Apalkov D, Dieny B, Slaughter JM (2016) Magnetoresistive random access memory. Proc IEEE 104(10):1796–1830. https://doi.org/10.1109/Jproc.2016.2590142

[88] Hsu J (2014) IBM's new brain. IEEE Spectr 51(10):17–19

[89] Yu SM, Chen HY, Gao B, Kang JF, Wong HSP (2013) HfOx-based vertical resistive switching random access memory suitable for bit-cost-effective three-dimensional

cross-point architecture. ACS Nano 7(3):2320–2325. https://doi.org/10.1021/nn305510u

[90] Zhang ZP, Wu Y, Wong HSP, Wong SS (2013) Nanometer-scale HfOx RRAM. IEEE Electron Dev Lett 34(8):1005–1007. https://doi.org/10.1109/Led.2013.2265404

[91] Yu SM, Gao B, Fang Z, Yu HY, Kang JF, Wong HSP (2013) Stochastic learning in oxide binary synaptic device for neuromorphic computing. Front Neurosci-Switz. https://doi.org/10.3389/fnins.2013.00186

[92] Gao B, Bi YJ, Chen HY, Liu R, Huang P, Chen B, Liu LF, Liu XY, Yu SM, Wong HSP, Kang JF (2014) Ultra-low-energy three-dimensional oxide-based electronic synapses for implementation of robust high-accuracy neuromorphic computation systems. ACS Nano 8(7):6998–7004. https://doi.org/10.1021/nn501824r

[93] Liu JC, Hsu CW, Wang IT, Hou TH (2015) Categorization of multilevel-cell storage-class memory: an RRAM example. IEEE Trans Electron Dev 62(8):2510–2516. https://doi.org/10.1109/Ted.2015.2444663

[94] Hsu CW, Hou TH, Chen MC, Wang IT, Lo CL (2013) Bipolar Ni/TiO2/HfO2/Ni RRAM with multilevel states and self-rectifying characteristics. IEEE Electron Device Lett 34(7):885–887. https://doi.org/10.1109/Led.2013.2264823

[95] Hou TH (2015) 3D RRAM-based synaptic network with low programming energy. In: 5th stanford-IMEC International RRAM Workshop, Leuven, Belgium, pp 24–25

[96] Burr GW, Shelby RM, Sebastian A, Kim S, Kim S, Sidler S, Virwani K, Ishii M, Narayanan P, Fumarola A, Sanches LL, Boybat I, Le Gallo M, Moon K, Woo J, Hwang H, Leblebici Y (2017) Neuromorphic computing using non-volatile memory. Adv Phys-X 2(1):89–124. https://doi.org/10.1080/23746149.2016.1259585

[97] Lee D, Park J, Moon K, Jang J-W, Park S, Chu M, Kim J, Noh J, Jeon M, Lee B, Lee B, Lee B-G, Hwang H (2015) Oxide based nanoscale analog synapse device for neural signal recognition system. In: Electron devices meeting (IEDM), 2015 IEEE international. https://doi.org/10.1109/iedm.2015.7409628

[98] Slutsky I, Abumaria N, Wu L-J, Huang C, Zhang L, Li B, Zhao X, Govindarajan A, Zhao M-G, Zhuo M, Tonegawa S, Liu G (2010) Enhancement of learning and memory by elevating brain magnesium. Neuron 65(2):165–177. https://doi.org/10.1016/j.neuron.2009.12.026

[99] Mayford M, Siegelbaum SA, Kandel ER (2012) Synapses and memory storage. Cold Spring Harb Perspect Biol 4(6):a005751. https://doi.org/10.1101/cshperspect.a005751

[100] Okano H, Hirano T, Balaban E (2000) Learning and memory. Proc Natl Acad Sci 97(23):12403–12404

[101] Shaw GL (1986) Donald Hebb: the organization of behavior. In: Palm G, Aertsen A (eds) Brain theory: proceedings of the first trieste meeting on brain theory, October 1–4, 1984. Springer, Berlin, pp 231–233. https://doi.org/10.1007/978-3-642-70911-1_15

[102] Bi GQ, Poo MM (1998) Synaptic modifications in cultured hippocampal neurons: dependence on spike timing, synaptic strength, and postsynaptic cell type. J Neurosci 18(24):10464–10472

[103] Zhang LI, Tao HW, Holt CE, Harris WA, Poo MM (1998) A critical window for cooperation and competition among developing retinotectal synapses. Nature 395(6697):37–44

[104] Markram H, Lubke J, Frotscher M, Sakmann B (1997) Regulation of synaptic efficacy by coincidence of postsynaptic APs and EPSPs. Science 275(5297):213–215. https://doi.org/10.1126/science.275.5297.213

[105] Ohno T, Hasegawa T, Tsuruoka T, Terabe K, Gimzewski JK, Aono M (2011) Short-term plasticity and long-term potentiation mimicked in single inorganic synapses. Nat Mater 10(8):591–595. https://doi.org/10.1038/Nmat3054

[106] Chen XR, Feng J, Ma HL (2015) The resistive switching characteristics in tantalum oxide-based RRAM device via combining high-temperature sputtering with plasma oxidation. In: 2015 15th non-volatile memory technology symposium (NVMTS)

[107] Li YY, Liu ZT, Tan TT (2014) Resistive switching behavior of hafnium oxide thin film grown by magnetron sputtering. Rare Metal Mat Eng 43(1):24–27

[108] Wu Y, Lee B, Wong H-SP (2010) Ultra-low power Al2O3-based RRAM with 1 μA reset current. In: VLSI technology systems and applications (VLSI-TSA), 2010 international symposium on

[109] Chang KC, Tsai TM, Chang TC, Syu YE, Chuang SL, Li CH, Gan DS, Sze SM (2012) The effect of silicon oxide based RRAM with tin doping. Electrochem Solid-State Lett 15(3):H65–H68. https://doi.org/10.1149/2.013203esl

[110] Wang SY, Tsai CH, Lee DY, Lin CY, Lin CC, Tseng TY (2011) Improved resistive switching properties of Ti/ZrO2/Pt memory devices for RRAM application. Microelectron Eng 88(7):1628–1632. https://doi.org/10.1016/j.mee.2010.11.058

[111] Liu KC, Tzeng WH, Chang KM, Wu CH (2010) The effect of plasma deposition on the electrical characteristics of Pt/HfOx/TiN RRAM device. Surf Coat Technol 205:S379–S384. https://doi.org/10.1016/j.surfcoat.2010.08.043

[112] Simanjuntak FM, Panda D, Tsai T-L, Lin C-A, Wei K-H, Tseng T-Y (2015) Enhancing the memory window of AZO/ZnO/ITO transparent resistive switching devices by modulating the oxygen vacancy concentration of the top

electrode. J Mater Sci 50(21):6961–6969. https://doi.org/10.1007/s10853-015-9247-y

[113] Wang J, Nonnenmann SS (2017) Area-dependent electroforming and switching polarity reversal across TiO2/Nb:SrTiO3 oxide interfaces. J Mater Sci 52(11):6469–6475. https://doi.org/10.1007/s10853-017-0882-3

[114] Wu Y, Lee B, Wong HSP (2010) Al2O3-Based RRAM using atomic layer deposition (ALD) with 1-mu a RESET current. IEEE Electron Device Lett 31(12):1449–1451. https://doi.org/10.1109/Led.2010.2074177

[115] Egorov KV, Lebedinskii YY, Markeev AM, Orlov OM (2015) Full ALD Ta2O5-based stacks for resistive random access memory grown with in vacuo XPS monitoring. Appl Surf Sci 356:454–459. https://doi.org/10.1016/j.apsusc.2015.07.217

[116] Sahu VK, Misra P, Ajimsha RS, Das AK, Joshi MP, Kukreja LM (2016) Resistive memory switching in ultrathin TiO2 films grown by atomic layer deposition. In: AIP conference proceedings vol 1731. https://doi.org/10.1063/1.4948104

[117] Niu G, Kim HD, Roelofs R, Perez E, Schubert MA, Zaumseil P, Costina I, Wenger C (2016) Material insights of HfO2-based integrated 1-transistor-1-resistor resistive random access memory devices processed by batch atomic layer deposition. Sci Rep. https://doi.org/10.1038/srep28155

[118] Misra P, Das AK, Kukreja LM (2010) Switching characteristics of ZnO based transparent resistive random access memory devices grown by pulsed laser deposition. Phys Status Solidi C 7(6):1718–1720. https://doi.org/10.1002/pssc.200983244

[119] Wu Z, Zhu J (2017) Enhanced unipolar resistive switching characteristics of Hf0.5Zr0.5O2 thin films with high ON/OFF ratio. Materials. https://doi.org/10.3390/ma10030322

[120] Parreira P, Paterson GW, McVitie S, MacLaren DA (2016) Stability, bistability and instability of amorphous ZrO2 resistive memory devices. J Phys D Appl Phys. https://doi.org/10.1088/0022-3727/49/9/095111

[121] Xu ZD, Yu LN, Wu Y, Dong C, Deng N, Xu XG, Miao J, Jiang Y (2015) Low-energy resistive random access memory devices with no need for a compliance current. Sci Rep. https://doi.org/10.1038/srep10409

[122] Hsu ST, Zhuang WW, Li TK, Pan W, Ignatiev A, Papagianni C, Wu NJ (2005) RRAM switching mechanism. In: 2005 Non-volatile memory technology symposium, proceedings, pp 121–124

[123] Preparation method of tungsten oxide variable-resistance material in resistive random access memory (2014) Google Patents

[124] Rodriguez R, Poulter B, Gonzalez M, Ali F, Lau LD, Mangun M (2017) The effect of tin on PECVD-deposited germanium sulfide thin films for resistive RAM devices. Mater Sci Appl 08:188–196

[125] Yao J, Sun ZZ, Zhong L, Natelson D, Tour JM (2010) Resistive switches and memories from silicon oxide. Nano Lett 10(10):4105–4110. https://doi.org/10.1021/nl102255r

[126] Mustaqima M, Yoo P, Huang W, Lee BW, Liu CL (2015) Regulation of the forming process and the set voltage distribution of unipolar resistance switching in spin-coated CoFe2O4 thin films. Nanoscale Res Lett. https://doi.org/10.1186/s11671-015-0876-5

[127] Xu HT, Wu CJ, Zhao XH, Jung RJ, Li Y, Liu CL (2017) Improved resistance switching stability in Fe-doped ZnO thin films through pulsed magnetic field annealing. Nanoscale Res Lett. https://doi.org/10.1186/s11671-017-1949-4

[128] Zhang F, Zhuang WW, Evans DR, Hsu ST (2004) High temperature annealing of spin coated Pr1-xCaxMnO3 thim film for RRAM application. Google patents

[129] Chang YC, Wei CY, Wang YH (2012) Sol-gel barium titanate-based RRAM by inserting graphene oxide interlayer. 2012 IEEE international conference on electron devices and solid state circuit (EDSSC)

[130] Wang Y, Chen B, Liu D, Gao B, Liu LF, Liu X, Kang J (2014) Solution processed resistive random access memory devices for transparent solid-state circuit systems. In: MRS online proceedings library archive, vol 1633. https://doi.org/10.1557/opl.2014.252

[131] Lee C, Kim I, Choi W, Shin H, Cho J (2009) Resistive switching memory devices composed of binary transition metal oxides using sol–gel chemistry. Langmuir 25(8):4274–4278

[132] Kim HD, Yun MJ, Lee JH, Kim KH, Kim TG (2014) Transparent multi-level resistive switching phenomena observed in ITO/RGO/ITO memory cells by the sol-gel dip-coating method. Sci Rep. https://doi.org/10.1038/srep04614

[133] Niu G, Calka P, Auf der Maur M, Santoni F, Guha S, Fraschke M, Hamoumou P, Gautier B, Perez E, Walczyk C, Wenger C, Di Carlo A, Alff L, Schroeder T (2016) Geometric conductive filament confinement by nanotips for resistive switching of HfO2-RRAM devices with high performance. Sci Rep 6:25757. https://doi.org/10.1038/srep25757

[134] Siddiqui G-U-D, Ali J, Doh Y-H, Choi KH (2016) Fabrication of zinc stannate based all-printed resistive switching device. Mater Lett 166(Supplement C):311–316. https://doi.org/10.1016/j.matlet.2015.12.045

[135] Asamitsu A, Tomioka Y, Kuwahara H, Tokura Y (1997) Current switching of resistive states in magnetoresistive manganites. Nature 388:50. https://doi.org/10.1038/40363

[136] Chen X, Wu NJ, Ignatiev A (2005) Perovskite RRAM devices with metal/insulator/PCMO/metal heterostructures. In: 2005 Non-volatile memory technology symposium, proceedings, pp 125–128

[137] Liu KC, Tzeng WH, Chang KM, Chan YC, Kuo CC, Cheng CW (2010) Transparent resistive random access memory (T-RRAM) based on Gd2O3 film and its resistive switching characteristics. In: INEC: 2010 3rd international nanoelectronics conference, vols 1 and 2, pp 898–899

[138] Park S, Kim H, Choo M, Noh J, Sheri A, Jung S, Seo K, Park J, Kim S, Lee W, Shin J, Lee D, Choi G, Woo J, Cha E, Jang J, Park C, Jeon M, Lee B, Lee BH, Hwang H (2012) RRAM-based synapse for neuromorphic system with pattern recognition function. In: 2012 IEEE international electron devices meeting (IEDM)

[139] Sangsu P, Jinwoo N, Myung-lae C, Ahmad Muqeem S, Man C, Young-Bae K, Chang Jung K, Moongu J, Byung-Geun L, Byoung Hun L, Hyunsang H (2013) Nanoscale RRAM-based synaptic electronics: toward a neuromorphic computing device. Nanotechnology 24(38):384009

[140] Park S, Sheri A, Kim J, Noh J, Jang J, Jeon M, Lee B, Lee BR, Lee BH, Hwang H (2013) Neuromorphic speech systems using advanced ReRAM-based synapse. In: 2013 IEEE international electron devices meeting (IEDM)

[141] Sangsu P, Manzar S, Jinwoo N, Daeseuk L, Kibong M, Jiyong W, Byoung HL, Hyunsang H (2014) A nitrogen-treated memristive device for tunable electronic synapses. Semicond Sci Technol 29(10):104006

[142] Moon K, Park S, Jang J, Lee D, Woo J, Cha E, Lee S, Park J, Song J, Koo Y, Hwang H (2014) Hardware implementation of associative memory characteristics with analogue-type resistive-switching device. Nanotechnology. https://doi.org/10.1088/0957-4484/25/49/495204

[143] Lee D, Moon K, Park J, Park S, Hwang H (2015) Trade-off between number of conductance states and variability of conductance change in Pr0.7Ca0.3MnO3-based synapse device. Appl Phys Lett. https://doi.org/10.1063/1.4915924

[144] Moon K, Cha E, Park J, Gi S, Chu M, Baek K, Lee B, Oh SH, Hwang H (2016) Analog synapse device with 5-b MLC and improved data retention for neuromorphic system. IEEE Electron Device Lett 37(8):1067–1070. https://doi.org/10.1109/Led.2016.2583545

[145] Moon K, Cha E, Lee D, Jang J, Park J, Hwang H (2016) ReRAM-based analog synapse and IMT neuron device for neuromorphic system. In: International symposium VLSI technology

[146] Yu S (2017) Neuro-inspired computing using resistive synaptic devices. Springer, Berlin

[147] Yu SM, Wu Y, Jeyasingh R, Kuzum DG, Wong HSP (2011) An electronic synapse device based on metal oxide resistive switching memory for neuromorphic computation. IEEE Trans Electron Dev 58(8):2729–2737. https://doi.org/10.1109/Ted.2011.2147791

[148] Gao B, Chen B, Zhang FF, Liu LF, Liu XY, Kang JF, Yu HY, Yu B (2013) A novel defect-engineering-based implementation for high-performance multilevel data storage in resistive switching memory. IEEE Trans Electron Dev 60(4):1379–1383. https://doi.org/10.1109/Ted.2013.2245508

[149] Garbin D, Vianello E, Bichler O, Rafhay Q, Gamrat C, Ghibaudo G, DeSalvo B, Perniola L (2015) HfO2-based OxRAM devices as synapses for convolutional neural networks. IEEE Trans Electron Dev 62(8):2494–2501. https://doi.org/10.1109/Ted.2015.2440102

[150] Benoist A, Blonkowski S, Jeannot S, Denorme S, Damiens J, Berger J, Candelier P, Vianello E, Grampeix H, Nodin JF, Jalaguier E, Perniola L, Allard B (2014) 28 nm Advanced CMOS resistive RAM solution as embedded non-volatile memory. In: International reliability physics symposium

[151] Guo T, Tan T, Liu Z (2015) The improved resistive switching of HfO2: Cu film with multilevel storage. J Mater Sci 50(21):7043–7047. https://doi.org/10.1007/s10853-015-9257-9

[152] Wang ZQ, Ambrogio S, Balatti S, Ielmini D (2015) A 2-transistor/1-resistor artificial synapse capable of communication and stochastic learning in neuromorphic systems. Front Neurosci-Switz. https://doi.org/10.3389/fnins.2014.00438

[153] Covi E, Brivio S, Fanciulli M, Spiga S (2015) Synaptic potentiation and depression in Al:HfO2-based memristor. Microelectron Eng 147:41–44. https://doi.org/10.1016/j.mee.2015.04.052

[154] Garbin D, Vianello E, Bichler O, Azzaz M, Rafhay Q, Candelier P, Gamrat C, Ghibaudo G, DeSalvo B, Pemiola L (2015) On the impact of OxRAM-based synapses variability on convolutional neural networks performance. In: IEEE international symposium nano, pp 193–198

[155] Lee MS, Lee JW, Kim CH, Park BG, Lee JH (2015) Implementation of short-term plasticity and long-term potentiation in a synapse using si-based type of charge-trap memory. IEEE Trans Electron Dev 62(2):569–573. https://doi.org/10.1109/Ted.2014.2378758

[156] Covi E, Brivio S, Serb A, Prodromakis T, Fanciulli M, Spiga S (2016) HfO2-based memristors for neuromorphic applications. IEEE International symposium on circuits

systems, pp 393–396. https://doi.org/10.1109/iscas.2016.7527253

[157] Werner T, Garbin D, Vianello E, Bichler O, Cattaert D, Yvert B, De Salvo B, Perniola L (2016) Real-time decoding of brain activity by embedded spiking neural networks using OxRAM synapses. In: IEEE international symposium on circuits systems, pp 2318–2321

[158] Werner T, Vianello E, Bichler O, Garbin D, Cattaert D, Yvert B, De Salvo B, Perniola L (2017) Spiking neural networks based on OxRAM synapses for real-time unsupervised spike sorting (vol 10, pg474, 2016). Front Neurosci-Switz. https://doi.org/10.3389/fnins.2017.00486

[159] Wang IT, Lin YC, Wang YF, Hsu CW, Hou TH (2014) 3D synaptic architecture with ultralow sub-10 fJ energy per spike for neuromorphic computation. In: 2014 IEEE international electron devices meeting (IEDM)

[160] Wang YF, Lin YC, Wang IT, Lin TP, Hou TH (2015) Characterization and modeling of nonfilamentary Ta/TaOx/TiO2/Ti analog synaptic device. Sci Rep. https://doi.org/10.1038/srep10150

[161] Wang IT, Chih-Cheng C, Li-Wen C, Teyuh C, Tuo-Hung H (2016) 3D Ta/TaO x/TiO 2/Ti synaptic array and linearity tuning of weight update for hardware neural network applications. Nanotechnology 27(36):365204

[162] Gao LG, Wang IT, Chen PY, Vrudhula S, Seo JS, Cao Y, Hou TH, Yu SM (2015) Fully parallel write/read in resistive synaptic array for accelerating on-chip learning. Nanotechnology. https://doi.org/10.1088/0957-4484/26/45/455204

[163] Wang ZW, Yin MH, Zhang T, Cai YM, Wang YY, Yang YC, Huang R (2016) Engineering incremental resistive switching in TaOx based memristors for brain-inspired computing. Nanoscale 8(29):14015–14022. https://doi.org/10.1039/c6nr00476h

[164] Wang Q, He DY (2017) Time-decay memristive behavior and diffusive dynamics in one forget process operated by a 3D vertical Pt/Ta2O5-x/W device. Sci Rep. https://doi.org/10.1038/s41598-017-00985-0

[165] Yao P, Wu HQ, Gao B, Eryilmaz SB, Huang XY, Zhang WQ, Zhang QT, Deng N, Shi LP, Wong HSP, Qian H (2017) Face classification using electronic synapses. Nat Commun. https://doi.org/10.1038/ncomms15199

[166] Yu SM, Gao B, Fang Z, Yu HY, Kang JF, Wong HSP (2012) A neuromorphic visual system using RRAM synaptic devices with sub-pJ energy and tolerance to variability: experimental characterization and large-scale modeling. In: 2012 IEEE international electron devices meeting (IEDM)

[167] Berdan R, Vasilaki E, Khiat A, Indiveri G, Serb A, Prodromakis T (2016) Emulating short-term synaptic dynamics with memristive devices. Sci Rep. https://doi.org/10.1038/srep18639

[168] Bousoulas P, Asenov P, Karageorgiou I, Sakellaropoulos D, Stathopoulos S, Tsoukalas D (2016) Engineering amorphous-crystalline interfaces in TiO2-x/TiO2-y-based bilayer structures for enhanced resistive switching and synaptic properties. J Appl Phys. https://doi.org/10.1063/1.4964872

[169] Mostafa H, Khiat A, Serb A, Mayr CG, Indiveri G, Prodromakis T (2015) Implementation of a spike-based perceptron learning rule using TiO(2 − x) memristors. Front Neurosci 9:357. https://doi.org/10.3389/fnins.2015.00357

[170] Park J, Kwak M, Moon K, Woo J, Lee D, Hwang H (2016) TiOx-based RRAM synapse with 64-levels of conductance and symmetric conductance change by adopting a hybrid pulse scheme for neuromorphic computing. IEEE Electron Device Lett 37(12):1559–1562. https://doi.org/10.1109/Led.2016.2622716

[171] Akoh N, Asai T, Yanagida T, Kawai T, Amemiya Y (2010) A ReRAM-based analog synaptic device having spike-timing-dependent plasticity. IEICE Tech Rep 110(246):23–28

[172] Hu SG, Liu Y, Chen TP, Liu Z, Yu Q, Deng LJ, Yin Y, Hosaka S (2013) Emulating the paired-pulse facilitation of a biological synapse with a NiOx-based memristor. Appl Phys Lett. https://doi.org/10.1063/1.4804374

[173] Hu SG, Liu Y, Liu Z, Chen TP, Yu Q, Deng LJ, Yin Y, Hosaka S (2014) Synaptic long-term potentiation realized in Pavlov's dog model based on a NiOx-based memristor. J Appl Phys. https://doi.org/10.1063/1.4902515

[174] Chang T, Jo SH, Kim KH, Sheridan P, Gaba S, Lu W (2011) Synaptic behaviors and modeling of a metal oxide memristive device. Appl Phys A-Mater 102(4):857–863. https://doi.org/10.1007/s00339-011-6296-1

[175] Fan-Yi M, Shu-Kai D, Li-Dan W, Xiao-Fang H, Zhe-Kang D (2015) An improved WOx memristor model with synapse characteristic analysis. Acta Phys Sinica 64(14):148501

[176] Yong Z, Yanling Y, Yuehua P, Weichang Z, Huajun Y, Zhu'ai Q, Binquan L, Yong Z, Dongsheng T (2014) Enhanced memristive performance of individual hexagonal tungsten trioxide nanowires by water adsorption based on Grotthuss mechanism. Mater Res Express 1(2):025025

[177] Prezioso M, Bayat FM, Hoskins B, Likharev K, Strukov D (2016) Self-adaptive spike-time-dependent plasticity of metal-oxide memristors. Sci Rep. https://doi.org/10.1038/srep21331

[178] Banerjee W, Liu Q, Lv H, Long S, Liu M (2017) Electronic imitation of behavioral and psychological synaptic activities using TiOx/Al2O3-based memristor devices. Nanoscale 9(38):14442–14450. https://doi.org/10.1039/C7NR04741J

[179] Wang CH, He W, Tong Y, Zhao R (2016) Investigation and manipulation of different analog behaviors of memristor as electronic synapse for neuromorphic applications. Sci Rep. https://doi.org/10.1038/srep22970

[180] Kim HJ, Zheng H, Park JS, Kim DH, Kang CJ, Jang JT, Kim DH, Yoon TS (2017) Artificial synaptic characteristics with strong analog memristive switching in a Pt/CeO2/Pt structure. Nanotechnology. https://doi.org/10.1088/1361-6528/aa712c

[181] Guo LQ, Wan Q, Wan CJ, Zhu LQ, Shi Y (2013) Short-term memory to long-term memory transition mimicked in IZO homojunction synaptic transistors. IEEE Electron Device Lett 34(12):1581–1583. https://doi.org/10.1109/Led.2013.2286074

[182] Chang YF, Fowler B, Chen YC, Zhou F, Pan CH, Chang TC, Lee JC (2016) Demonstration of synaptic behaviors and resistive switching characterizations by proton exchange reactions in silicon oxide. Sci Rep. https://doi.org/10.1038/srep21268

[183] Driscoll T, Palit S, Qazilbash MM, Brehm M, Keilmann F, Chae B-G, Yun S-J, Kim H-T, Cho SY, Jokerst NM, Smith DR, Basov DN (2008) Dynamic tuning of an infrared hybrid-metamaterial resonance using vanadium dioxide. Appl Phys Lett 93(2):024101. https://doi.org/10.1063/1.2956675

[184] Driscoll T, Kim H-T, Chae B-G, Kim B-J, Lee Y-W, Jokerst NM, Palit S, Smith DR, Di Ventra M, Basov DN (2009) memory metamaterials. Science 325(5947):1518–1521. https://doi.org/10.1126/science.1176580

[185] Lee MJ, Park Y, Suh DS, Lee EH, Seo S, Kim DC, Jung R, Kang BS, Ahn SE, Lee CB, Seo DH, Cha YK, Yoo IK, Kim JS, Park BH (2007) Two series oxide resistors applicable to high speed and high density nonvolatile memory. Adv Mater 19(22):3919–3923. https://doi.org/10.1002/adma.200700251

[186] Son M, Lee J, Park J, Shin J, Choi G, Jung S, Lee W, Kim S, Park S, Hwang H (2011) Excellent selector characteristics of nanoscale VO2 for high-density bipolar ReRAM applications. IEEE Electron Device Lett 32(11):1579–1581. https://doi.org/10.1109/LED.2011.2163697

[187] Zhang K, Wang B, Wang F, Han Y, Jian X, Zhang H, Wong HSP (2016) VO2-based selection device for passive resistive random access memory application. IEEE Electron Device Lett 37(8):978–981. https://doi.org/10.1109/LED.2016.2582259

[188] Krzysteczko P, Munchenberger J, Schafers M, Reiss G, Thomas A (2012) The memristive magnetic tunnel junction as a nanoscopic synapse-neuron system. Adv Mater 24(6):762–766. https://doi.org/10.1002/adma.201103723

[189] Yoshida C, Tsunoda K, Noshiro H, Sugiyama Y (2007) High speed resistive switching in Pt/TiO2/TiN film for nonvolatile memory application. Appl Phys Lett 91(22):223510. https://doi.org/10.1063/1.2818691

[190] Yoshida C, Kinoshita K, Yamasaki T, Sugiyama Y (2008) Direct observation of oxygen movement during resistance switching in NiO/Pt film. Appl Phys Lett 93(4):042106. https://doi.org/10.1063/1.2966141

[191] Huang Y-C, Chen P-Y, Chin T-S, Liu R-S, Huang C-Y, Lai C-H (2012) Improvement of resistive switching in NiO-based nanowires by inserting Pt layers. Appl Phys Lett 101(15):153106. https://doi.org/10.1063/1.4758482

[192] Chien WC, Lee MH, Feng-Ming L, Lin YY, Hsiang-Lan L, Hsieh KY, Chih-Yuan L (2011) Multi-level 40 nm WOX resistive memory with excellent reliability. In: 2011 International electron devices meeting, 5–7 Dec. 2011 2011. pp 313531–313534. https://doi.org/10.1109/iedm.2011.6131651

[193] Chao X, Biao N, Long Z, Long-Hui Z, Yong-Qiang Y, Xian-He W, Qun-Ling F, Lin-Bao L, Yu-Cheng W (2013) High-performance nonvolatile Al/AlO x/CdTe: Sb nanowire memory device. Nanotechnology 24(35):355203

[194] Chih Yang Lina CYW, Wua Chung Yi, Hub Chenming, Tseng Tseung Yuen (2007) Bistable resistive switching in Al2O3 memory thin films. J Electrochem Soc. https://doi.org/10.1149/1.2750450

[195] Zhu W, Chen TP, Yang M, Liu Y, Fung S (2012) Resistive Switching Behavior of Partially Anodized Aluminum Thin Film at Elevated Temperatures. IEEE Trans Electron Devices. https://doi.org/10.1109/TED.2012.2205692

[196] Chen YS, Chen B, Gao B, Zhang FF, Qiu YJ, Lian GJ, Liu LF, Liu XY, Han RQ, Kang JF (2010) Anticrosstalk characteristics correlated with the set process for α-Fe2O3/Nb–SrTiO3 stack-based resistive switching device. Appl Phys Lett 97(26):262112. https://doi.org/10.1063/1.3532970

[197] Muraoka S, Osano K, Kanzawa Y, Mitani S, Fujii S, Katayama K, Katoh Y, Wei Z, Mikawa T, Arita K, Kawashima Y, Azuma R, Kawai K, Shimakawa K, Odagawa A, Takagi T (2007) Fast switching and long retention Fe-O ReRAM and its switching mechanism. In: 2007 IEEE international electron devices meeting, 10–12 Dec. 2007. pp 779–782. https://doi.org/10.1109/iedm.2007.4419063

[198] Dou C, Kakushima K, Ahmet P, Tsutsui K, Nishiyama A, Sugii N, Natori K, Hattori T, Iwai H (2012) Resistive switching behavior of a CeO2 based ReRAM cell incorporated with Si buffer layer. Microelectron Reliab 52(4):688–691. https://doi.org/10.1016/j.microrel.2011.10.019

[199] Lee D, D-j Seong, Jo I, Xiang F, Dong R, Oh S, Hwang H (2007) Resistance switching of copper doped MoOx films

for nonvolatile memory applications. Appl Phys Lett 90(12):122104. https://doi.org/10.1063/1.2715002

[200] Li Y, Sinitskii A, Tour JM (2008) Electronic two-terminal bistable graphitic memories. Nat Mater 7:966. https://doi.org/10.1038/nmat2331

[201] Syu YE, Zhang R, Chang TC, Tsai TM, Chang KC, Lou JC, Young TF, Chen JH, Chen MC, Yang YL, Shih CC, Chu TJ, Chen JY, Pan CH, Su YT, Huang HC, Gan DS, Sze SM (2013) Endurance improvement technology with nitrogen implanted in the interface of WSiOx resistance switching device. IEEE Electron Device Lett 34(7):864–866. https://doi.org/10.1109/LED.2013.2260125

[202] Yu D, Liu LF, Chen B, Zhang FF, Gao B, Fu YH, Liu XY, Kang JF, Zhang X (2011) Multilevel resistive switching characteristics in Ag/SiO2/Pt RRAM devices. In: 2011 IEEE international conference of electron devices and solid-state circuits, 17–18 Nov. 2011. pp 1–2. https://doi.org/10.1109/edssc.2011.6117721